A Multi-objective Chance-constrained Information-gap Decision Model for Active Management to Accommodate Multiple Uncertainties in Distribution Networks

Shida Zhang, Shaoyun Ge, Hong Liu, Junkai Li, Chenghong Gu, and Chengshan Wang

***Abstract*—The load demand and distributed generation (DG) integration capacity in distribution networks (DNs) increase constantly, and it means that the violation of security constraints may occur in the future. This can be further worsened by short-term power fluctuations. In this paper, a scheduling method based on a multi-objective chance-constrained information-gap decision (IGD) model is proposed to obtain the active management schemes for distribution system operators (DSOs) to address these problems. The maximum robust adaptability of multiple uncertainties, including the deviations of growth prediction and their relevant power fluctuations, can be obtained based on the limited budget of active management. The systematic solution of the proposed model is developed. The max term constraint in the IGD model is converted into a group of normal constraints corresponding to extreme points of the max term. Considering the stochastic characteristics and correlations of power fluctuations, the original model is equivalently reformulated by using the properties of multivariate Gaussian distribution. The effectiveness of the proposed model is verified by a modified IEEE 33-bus distribution network. The simulation result delineates a robust accommodation space to represent the adaptability of multiple uncertainties, which corresponds to an optional active management strategy set for future selection.**

***Index Terms*—Active management, distribution network, multiple uncertainties, information gap decision theory, chance constraint.**

NOMENCLATURE

A. Indices

i, j, k	Index of buses
ij	Index of branches
t	Index of periods

B. Sets

Ω_{α}	Robust accommodation space about (α_{L}, α_{DG})
Ω_{φ}	Robust accommodation space about (φ_{L}, φ_{DG})
Ω_{bus}, Ω_{branch}, Ω_{SUB}	Sets of buses, branches, and substations
Ω_{cb}	Set of capacitor banks
Ω_{rcs}	Set of remotely controlled switches
Ω_{T}	Set of periods
Ω_{Y}	Set of days in one year
U_{L}, U_{DG}	Information gaps of loads and DGs

C. Parameters

$\bar{\delta}^{\mathrm{re}}_{i,\max}$	Limitation of reduction rate at bus i
$\underline{\delta}^{\mathrm{trans}}_{i,\min}$, $\bar{\delta}^{\mathrm{trans}}_{i,\max}$	Lower and upper limits of transfer rate at bus i
v	Increase of the active management cost
$\rho_{\mathrm{cur},ij,t}$	Correlation coefficient between DG curtailment at buses i and j during period t
$\rho_{\mathrm{DG},ij,t}$	Correlation coefficient between DGs at buses i and j during period t
$\rho^{\mathrm{PQ}}_{\mathrm{L},i,t}$	Correlation coefficient between active and reactive power components of load demand at buses i during period t
$\rho^{\mathrm{P}}_{\mathrm{L},ij,t}$, $\rho^{\mathrm{Q}}_{\mathrm{L},ij,t}$	Correlation coefficients between acitve and reactive load demands at buses i and j during period t
$\rho_{\mathrm{trans},ij,t}$, $\rho_{\mathrm{re},ij,t}$	Correlation coefficients between transferable and reducible loads at buses i and j during period t
σ_{cur}	Standard deviation coefficient of unpredictable response of DG curtailment
σ_{L}, σ_{DG}	Standard deviation coefficients of prediction error in loads and DGs
σ_{trans}, σ_{re}	Standard deviation coefficients of unpredictable response of transferable and reducible loads

Manuscript received: April 2, 2022; revised: July 20, 2022; accepted: September 5, 2022. Date of CrossCheck: September 5, 2022. Date of online publication: October 27, 2022.

This work was supported by the National Natural Science Foundation of China (No. U1866207).

S. Zhang, S. Ge, H. Liu (corresponding author), J. Li, and C. Wang are with the School of Electrical and Information Engineering, Tianjin University, Tianjin 300072, China (e-mail: zhangshida@tju.edu.cn; syge@tju.edu.cn; liuhong@tju.edu.cn; lijunkai6666@tju.edu.cn; cswang@tju.edu.cn).

C. Gu is with the Department of Electrical and Electronic Engineering, University of Bath, Bath BA2 7AY, U.K. (e-mail: c.gu@bath.ac.uk).

DOI: 10.35833/MPCE.2022.000193

ϕ_{DG} Power-factor angle of DGs

$C_{\mathrm{price}}^{\mathrm{cb}}$ Price of a single action of capacitor bank

$C_{\mathrm{dev}}^{\mathrm{cur}}$ Annual cost of DG curtailment device for unit capacity

$C_{\mathrm{price}}^{\mathrm{cur}}$ Price of DG curtailment for unit power

$C_{\mathrm{price}}^{\mathrm{nr}}$ Price of a single action of remotely controlled switch in network reconfiguration

$C_{\mathrm{dev}}^{\mathrm{trans}}$, $C_{\mathrm{dev}}^{\mathrm{re}}$ Annual costs of transferable and reducible load device for unit capacity

$C_{\mathrm{price}}^{\mathrm{trans}}$, $C_{\mathrm{price}}^{\mathrm{re}}$ Incentive prices of transferable load and reducible load for unit power

M_1, M_2, M_3, M_4 Big-M parameters

N Number of buses

$N_i^{\mathrm{cb,daily}}$ Daily allowable number of capacitor bank actions at bus i

$N_i^{\mathrm{cb,max}}$ The maximum capacitor bank numbers at bus i

$N_{\mathrm{max}}^{\mathrm{trans}}$, $N_{\mathrm{max}}^{\mathrm{re}}$ The maximum numbers of buses allowed to implement transferring and reduction

$P_{\mathrm{DG},i,t}^{\mathrm{pre}}$, $Q_{\mathrm{DG},i,t}^{\mathrm{pre}}$, Predicted DG active and reactive outputs at bus i during period t

$P_{\mathrm{L},i,t}^{\mathrm{pre}}$, $Q_{\mathrm{L},i,t}^{\mathrm{pre}}$ Predicted active and reactive load demands at bus i during period t

$P_{\mathrm{L},i}^{\mathrm{pre,max}}$, $P_{\mathrm{DG},i}^{\mathrm{pre,max}}$ The largest active load demand and DG output at bus i

p_{V}, p_{S}, p_{SUB} Allowing violation probability of voltage constraints, branch thermal constraints, and substation capacity constraints

$Q_i^{\mathrm{cb,unit}}$ Unit reactive power of capacitor bank at bus i

R_{ij}, X_{ij} Resistance and reactance at branch ij

$S_{ij,\mathrm{max}}$ The maximum capacity of the branch at branch ij

$S_{i,\mathrm{max}}^{\mathrm{SUB}}$ The maximum capacity of the substation at bus i

V_{min}, V_{max} Lower and upper limits of bus voltage

Δt Dispatch period

D. Functions

$\boldsymbol{\Phi}$, $\boldsymbol{\Phi}$ Standardized Gaussian distribution and its vector form

$E_{\mathrm{p}}(\cdot)$ Mathematical expectation

$\mathcal{N}_{\mathrm{bivariate}}(\cdot)$ Bivariate Gaussian distribution

$\mathcal{N}_{2N}(\cdot)$ 2N-dimensional multivariate Gaussian distribution

E. Binary Variables

$\beta_{i,t}^{\mathrm{cb}}$ Capacitor bank used at bus i during period t

$\beta_{ij,t}^{\mathrm{nr}}$ Switching action at branch ij during period t

$\delta_{i,t}^{\mathrm{cb,in}}$, $\delta_{i,t}^{\mathrm{cb,de}}$ Decisions about capacitor bank increase or decrease at bus i during period t

y_i Decision about whether to implement load transferring at bus i

z_i Decision about whether to implement load reduction at bus i

F. Continuous Variables

α_{L}, α_{DG} The maximum deviations between actuality and prediction in loads and DGs

$\overline{\delta}_i^{\mathrm{cur}}$ Scheme of the maximum curtailment rate at bus i

$\overline{\delta}_i^{\mathrm{re}}$ Scheme of the maximum reduction rate at bus i

$\overline{\delta}_i^{\mathrm{trans}}$, $\underline{\delta}_i^{\mathrm{trans}}$ Scheme of transferring range of transferable load at bus i

$\theta_{i,t}$, $V_{i,t}$ Voltage angle and magnitude at bus i during period t

$\lambda_{\mathrm{Vmax},i,t}$, $\lambda_{\mathrm{Vmin},i,t}$, $\lambda_{\mathrm{Pmax},i,t}$, $\lambda_{\mathrm{Pmin},i,t}$, $\lambda_{\mathrm{Qmax},i,t}$, $\lambda_{\mathrm{Qmin},i,t}$, $\lambda_{\mathrm{P+Qmax},i,t}$, $\lambda_{\mathrm{P+Qmin},i,t}$, $\lambda_{\mathrm{P-Qmax},i,t}$, $\lambda_{\mathrm{P-Qmin},i,t}$ Auxiliary variables

$\boldsymbol{\mu}_{\mathrm{P},t}$, $\boldsymbol{\mu}_{\mathrm{Q},t}$ Expectation vectors of active and reactive injections during period t

$\boldsymbol{\mu}_{\theta,t}$, $\boldsymbol{\mu}_{\mathrm{V},t}$ Expectation vectors of voltage angles and amplitudes during period t

$\boldsymbol{\Sigma}_t^{\mathrm{DG}}$ Covariance matrix of active power of DG outputs during period t

$\boldsymbol{\Sigma}_t^{\mathrm{L,P}}$, $\boldsymbol{\Sigma}_t^{\mathrm{L,Q}}$, $\boldsymbol{\Sigma}_t^{\mathrm{L,PQ}}$ Covariance matrices of active and reactive load demands during period t

$\boldsymbol{\Sigma}_{\mathrm{P},t}$, $\boldsymbol{\Sigma}_{\mathrm{Q},t}$, $\boldsymbol{\Sigma}_{\mathrm{PQ},t}$ Covariance matrices of active and reactive injections during period t

$\boldsymbol{\Sigma}_t^{\mathrm{trans}}$, $\boldsymbol{\Sigma}_t^{\mathrm{re}}$ Covariance matrices of active power of transferable and reducible loads during period t

$\boldsymbol{\Sigma}_t^{\mathrm{cur}}$ Covariance matrix of active power of DG curtailment during period t

$\boldsymbol{\Sigma}_{\theta,t}$, $\boldsymbol{\Sigma}_{\mathrm{V},t}$, $\boldsymbol{\Sigma}_{\theta\mathrm{V},t}$ Covariance matrices of voltage angles and amplitudes during period t

φ_{L}, φ_{DG} Proportions of actuality to prediction during loads and DGs

C_{cb} Total cost of capacitor bank actions

C_{cur} Total cost of DG curtailment

C_{loss} Annual energy loss cost of distribution network

C_{nr} Total cost of network reconfiguration

C_{trans}, C_{re} Total costs of transferable loads and reducible loads

F_{AM} Annual active management cost

$l_{ij,t}$, $v_{i,t}$ Square of branch currents and bus voltage at branch ij during period t

$P_{i,t}$, $Q_{i,t}$ Active and reactive power of injection at bus i during period t

$P_{ij,t}$, $Q_{ij,t}$ Active and reactive power at branch ij during period t

$P_{i,t}^{\mathrm{cur}}$, $Q_{i,t}^{\mathrm{cur}}$ Active and reactive power of DG curtailment at bus i during period t

$P_{i,t}^{\mathrm{re}}$, $Q_{i,t}^{\mathrm{re}}$ Active and reactive power of reducible load at bus i during period t

$P_{i,t}^{\mathrm{SUB}}$, $Q_{i,t}^{\mathrm{SUB}}$ Active and reactive power injection at substation i during period t

$P_{i,t}^{\mathrm{trans}}$, $Q_{i,t}^{\mathrm{trans}}$ Transferring active and reactive power of transferable load at bus i during period t

$Q_{i,t}^{\mathrm{cb}}$ Reactive power of capacitor bank at bus i during period t

U_{L}, U_{DG} Information gap of load growth and DG integration capacity growth

$\boldsymbol{u}$ A vector of all active management decision variables

G. Random Variables

$\tilde{\theta}_{i,t}$, $\tilde{V}_{i,t}$ Voltage angle and magnitude considering uncertainty at bus i during period t

$\tilde{P}_{\mathrm{DG},i,t}$, $\tilde{Q}_{\mathrm{DG},i,t}$ $\tilde{P}_{\mathrm{L},i,t}$, $\tilde{Q}_{\mathrm{L},i,t}$ Active and reactive power of DG output and load demand considering uncertainty at bus i during period t

$\tilde{P}_{i,t}$, $\tilde{Q}_{i,t}$ Active and reactive power of injection considering uncertainty at bus i during period t

$\tilde{P}_{ij,t}$, $\tilde{Q}_{ij,t}$ Active and reactive power considering uncertainty at branch ij during period t

$\tilde{P}_{i,t}^{\mathrm{cur}}$, $\tilde{Q}_{i,t}^{\mathrm{cur}}$, $\tilde{P}_{i,t}^{\mathrm{re}}$, $\tilde{Q}_{i,t}^{\mathrm{re}}$, $\tilde{P}_{i,t}^{\mathrm{trans}}$, $\tilde{Q}_{i,t}^{\mathrm{trans}}$ Active and reactive power of DG curtailment, reducible load, and transferable load considering uncertainty at bus i during period t

$\tilde{P}_{i,t}^{\mathrm{SUB}}$, $\tilde{Q}_{i,t}^{\mathrm{SUB}}$ Active and reactive power of injection considering uncertainty at substation i during period t

I. Introduction

With technological progress and social development, the load demand and distributed generation (DG) integration capacity in distribution networks (DNs) increase constantly, and it means that the violation of security constraints (such as bus voltage constraints and branch thermal constraints) may occur in the future. Moreover, short-term power fluctuations of DGs and loads may result in a worse scenario for the stable operation of DNs. All these will bring significant challenges to distribution system operators (DSOs).

To tackle these difficulties, active management is one of the effective methods, which has been widely used in optimal DN scheduling [1], [2]. Many active management methods such as demand response (DR) [3], [4], DG curtailment [5], reactive power compensation, and network reconfiguration, are effective for improving the controllability of DNs and mitigating security violations [6], [7]. There are various kinds of demand-side resources [8], [9] in DNs that have different response characteristics such as reducible load [10] and transferable load [11]. DG output curtailment [5] is a significant measure of active management on the supply side because it can alleviate over-voltage problems during peak power periods. Capacitor bank (CB) is a classic and efficient reactive power compensation equipment to address low-voltage issues [2]. Dynamic network reconfiguration based on remotely controlled switches (RCSs) [12] can remove grid congestions in real time, and maintain branch thermal constraints.

Therefore, DSOs may seek optimal dispatch schemes of active management elements to address the security violation problem in various future scenarios. The main uncertainties of the future scenarios in DNs include short-term power fluctuations and long-term deviations of growth prediction.

Many studies propose the methods to address the uncertainties of intraday/day-ahead instantaneous power fluctuation and prediction errors of DGs and loads [13], [14] as well as the uncertainties of demand-side resources [15]. Modeling this kind of uncertainty as random variables is an effective method which describes stochastic characteristics with probabilistic density functions (PDFs) [14].

Scenario-based stochastic programming [14], [16] and chance-constrained programming (CCP) [17], [18] are widely used to formulate optimization problems with random variables. The scenario-based method considers possible realizations via typical scenarios that can be derived from certain empirical PDFs or data-driven discrete probability distributions. Reference [16] used a scenario-based method to obtain the optimal scheduling of DR in pre-emptive markets. However, the performance of scenario-based methods is usually restricted by the scale of scenarios, but a considerable number of scenarios will increase the complexity of the calculation.

CCP requires that constraints hold with a certain probability [18]. For active management decisions, [15] proposed a distributionally robust chance constraint formulation of the frequency metrics to account for the uncertainty associated with noncritical load shedding, and the chance constraints are further effectively reformulated into second-order cone (SOC) form. Reference [19] proposed a chance-constrained model to find the optimal high-voltage alternating current (HVAC) operation schedule against the stochastic nature of electricity prices, solar power generations, and weather conditions. The model was solved based on a sampling-based method. Reference [20] modeled the stochastic controllability of DR resources in a unit commitment problem, and chance constraints were analytically reformulated as SOC constraints with high computational efficiency. But the correlation between random variables was not considered in [20]. It is significant to enhance other uncertainty addressing methods by combining chance constraints. In this way, the comprehensive characteristics of uncertainties can be considered.

Apart from power fluctuations, growth uncertainties in DGs and loads are essential. However, the method based on random variables cannot perform excellently in modeling growth uncertainties because they could be impacted by numerous potential influencing factors such as economic development and government policies [10], [17].

Information-gap decision theory (IGDT) does not need to model the uncertain factor in a definite form. The essence of IGDT is to obtain the maximum accommodation (defined as information gaps) of uncertain factors with restricted resources. Therefore, this is more appropriate for assessing the adaptability of growth uncertainties. In the practical program, the budget of distribution system operators (DSOs) for an engineering target is usually finite. IGDT-based methods can provide a series of schemes within a limited budget, which means that IGDT is more suitable for engineering practices.

In the aspect of planning, IGDT has been applied in microgrid design [17], DN reinforcement [21], [22], etc. From an operation perspective, information-gap decision (IGD) models are formulated to tackle the optimal power flow (OPF) of high-voltage direct current (HVDC) system [23], unit commitment [24], DR trading strategies [10], virtual power plant scheduling [25], etc. Reference [17] proposed an IGDT-based multi-period planning framework combined with chance constraints. The authors addressed short-term uncertainty (such as fluctuations of DG output) with chance constraints and long-term uncertainty (such as load demand growth) with IGDT. However, multiple long-term uncertainties such as the growth of DGs and loads could not be considered simultaneously in this framework.

Furthermore, it is difficult to solve the max/min term in the constraint of the IGD model [10]. References [21] and [23] simplified the max/min term by discussing the conditions of optimization. References [10], [17], [22] obtained the expression of the max/min term in the constraint by identifying the monotonic relationship between uncertain factors and the robust/opportunistic function. In [25], the max/min term constraints were mathematically transformed as nonconvex additional constraints under the certain principles. Nevertheless, these methods depend on apriori knowledge, which may be difficult to implement when multiple uncertainties are considered and the monotonic relationships are not clear. Therefore, a tractable solving method for IGD models without apriori knowledge needs further research.

A comparison between recent studies and proposed method about IGDT is provided in Table I, which includes objective function, solution, and combination with other uncertainty addressing methods.

TABLE I
COMPARISON BETWEEN RECENT STUDIES AND PROPOSED METHOD ABOUT IGDT

Reference	Objective function		Solution		Combination with other uncertainty addressing methods	
	Single objective	Multiple objectives	Requiring apriori knowledge	Not requiring apriori knowledge	Combining but not considering correlations	Combining and considering correlations
[10]		√	√			
[17]	√		√		√	
[21], [23]-[25]	√		√			
[22]		√	√			
This paper		√		√		√

In this paper, an active management decision method based on a multi-objective chance-constrained IGD model is proposed to obtain the active management schemes (including DR, DG curtailment, reactive power compensation, and network reconfiguration) for DSOs. It aims to address the security violation problem in various future scenarios of DGs and loads. The main contributions of this paper can be summarized as follows.

1) It proposes a multi-objective chance-constrained IGD model for active management. The maximum robust adaptability of multiple uncertainties, including deviations of growth prediction and power fluctuations, can be obtained based on the limited budget of active management. The deviations of growth prediction in loads and DGs are formulated as information gaps. To reflect the impact of short-term power fluctuations under growth deviations, the chance constraints are formulated to ensure the validity of operation security constraints.

2) The systematic solution of the proposed model is developed. Based on the linearized power flow and linear programming theory, the max term constraint is transformed into a group of normal constraints corresponding to extreme points of the max term. Then, the stochastic characteristics and correlations of power fluctuations in DGs, loads, and active management elements are adequately considered using the properties of the multivariate Gaussian distribution. As a result, the original model is reformulated as a tractable multi-objective problem, which can be solved directly by the ε constraint algorithm.

3) The maximum robust accommodation space of multiple uncertainties is obtained. Each point in the space indicates an adaptable realization of uncertainties and relates to a scheduling scheme under the budget. Therefore, an optional scheduling strategy set can be constructed. DSOs can flexibly select the active management scheme from the set against the actual scenario in the future as long as the scenario is in the robust accommodation space.

The rest of this paper is organized as follows. Section II introduces the models of loads, DGs, and active management means with multiple uncertainties. The active management decision method based on the chance-constrained IGD model is proposed in Section III. Section IV presents the solving method of the proposed model. Section V presents case study to verify the effectiveness of the proposed model by a modified IEEE 33-bus DN. Section VI concludes the work in this paper.

II. Models of Loads, DGs, and Active Management Means with Multiple Uncertainties

This section models load demands, DG outputs, and active management measures. Power fluctuations and deviations of growth prediction are analyzed, respectively.

A. Load Demands

1) Power Fluctuation

Random variables are usually used to describe power fluctuations. In this paper, random errors are added to the time-series curves of prediction loads in the future scenario to represent power fluctuations. The demand load at node i during period t is formulated as a bivariate Gaussian distribution [26] to consider the correlation between active and reactive power, which is shown in (1).

$$\left(\tilde{P}_{\mathrm{L},i,t},\tilde{Q}_{\mathrm{L},i,t}\right): \mathcal{N}_{\mathrm{bivariate}}\left(P^{\mathrm{pre}}_{\mathrm{L},i,t},Q^{\mathrm{pre}}_{\mathrm{L},i,t},\left(\sigma^{\mathrm{P}}_{\mathrm{L}}P^{\mathrm{pre}}_{\mathrm{L},i,t}\right)^2,\left(\sigma^{\mathrm{Q}}_{\mathrm{L}}Q^{\mathrm{pre}}_{\mathrm{L},i,t}\right)^2,\rho^{\mathrm{PQ}}_{\mathrm{L},i,t}\right) \tag{1}$$

Coefficient $\rho^{\mathrm{PQ}}_{\mathrm{L},i,t}$ reveals the correlation between load demands $\tilde{P}_{\mathrm{L},i,t}$ and $\tilde{Q}_{\mathrm{L},i,t}$.

The correlation between load demands at bus i and bus j can be formulated by bivariate Gaussian distributions as follows.

$$\begin{cases}\left(\tilde{P}_{\mathrm{L},i,t},\tilde{P}_{\mathrm{L},j,t}\right): \\ \quad \mathcal{N}_{\mathrm{bivariate}}\left(P^{\mathrm{pre}}_{\mathrm{L},i,t},P^{\mathrm{pre}}_{\mathrm{L},j,t},\left(\sigma^{\mathrm{P}}_{\mathrm{L}}P^{\mathrm{pre}}_{\mathrm{L},i,t}\right)^2,\left(\sigma^{\mathrm{P}}_{\mathrm{L}}P^{\mathrm{pre}}_{\mathrm{L},i,t}\right)^2,\rho^{\mathrm{P}}_{\mathrm{L},ij,t}\right) \\ \left(\tilde{Q}_{\mathrm{L},i,t},\tilde{Q}_{\mathrm{L},j,t}\right): \\ \quad \mathcal{N}_{\mathrm{bivariate}}\left(Q^{\mathrm{pre}}_{\mathrm{L},i,t},Q^{\mathrm{pre}}_{\mathrm{L},j,t},\left(\sigma^{\mathrm{Q}}_{\mathrm{L}}Q^{\mathrm{pre}}_{\mathrm{L},i,t}\right)^2,\left(\sigma^{\mathrm{Q}}_{\mathrm{L}}Q^{\mathrm{pre}}_{\mathrm{L},i,t}\right)^2,\rho^{\mathrm{Q}}_{\mathrm{L},ij,t}\right)\end{cases} \quad \forall i,j,\forall t \tag{2}$$

Coefficients $\rho^{\mathrm{P}}_{\mathrm{L},ij,t}$ and $\rho^{\mathrm{Q}}_{\mathrm{L},ij,t}$ reveal the correlations between load demands in different buses.

By combining (1) and (2) into matrix form, all loads during each period follow the $2N$-dimensional multivariate Gaussian distribution in (3).

$$\begin{bmatrix}\tilde{\boldsymbol{P}}_{\mathrm{L},t}\\ \tilde{\boldsymbol{Q}}_{\mathrm{L},t}\end{bmatrix}=\mathcal{N}_{2N}\left(\begin{bmatrix}\boldsymbol{P}^{\mathrm{pre}}_{\mathrm{L},t}\\ \boldsymbol{Q}^{\mathrm{pre}}_{\mathrm{L},t}\end{bmatrix},\begin{bmatrix}\boldsymbol{\Sigma}^{\mathrm{L,P}}_{t} & \boldsymbol{\Sigma}^{\mathrm{L,PQ}}_{t}\\ \boldsymbol{\Sigma}^{\mathrm{L,QP}}_{t} & \boldsymbol{\Sigma}^{\mathrm{L,Q}}_{t}\end{bmatrix}\right) \quad \forall t \tag{3}$$

The expressions of covariance matrices $\boldsymbol{\Sigma}^{\mathrm{L,P}}_{t}$, $\boldsymbol{\Sigma}^{\mathrm{L,Q}}_{t}$, and $\boldsymbol{\Sigma}^{\mathrm{L,PQ}}_{t}$ are shown in Appendix A (A1)-(A3).

2) Deviation of Growth Prediction

The growth of load demands is influenced by numerous factors such as economic development and government policies. There may be an uncertain gap between prediction value and actual value in the future. This kind of uncertain factor is defined as the deviation of growth prediction, which is challenging to address precisely. To model the prediction error, an envelope-bound uncertainty method [10] is employed in this paper to model the uncertain factors in IGDT.

$$U_{\mathrm{L}}\left(\alpha_{\mathrm{L}},\varphi_{\mathrm{L}}\right)=\left\{\varphi_{\mathrm{L}}:\left|\varphi_{\mathrm{L}}-1\right|\le\alpha_{\mathrm{L}};\alpha_{\mathrm{L}}\ge 0;\varphi_{\mathrm{L}}\in\left[\left(1-\alpha_{\mathrm{L}}\right),\left(1+\alpha_{\mathrm{L}}\right)\right]\right\} \tag{4}$$

The envelope-bound uncertainty set (4), which is defined as information gap U_{L}, is used to represent the uncertainty of load growth. The proportion of actuality to prediction φ_{L}, which indicates the proportion of actuality to prediction in loads, is a realization of U_{L} and represents a future scenario of load growth. α_{L} is the width of the information gap, which indicates the maximum deviation between the actuality and prediction.

B. DG Outputs

1) Power Fluctuation

Assuming that the power factor of DG outputs $\cos\phi_{\mathrm{DG}}$ remains the same, the DG outputs considering the correlation can be modeled as follows.

$$\begin{cases}\left(\tilde{P}_{\mathrm{DG},i,t},\tilde{P}_{\mathrm{DG},j,t}\right): \\ \quad \mathcal{N}_{\mathrm{bivariate}}\left(P^{\mathrm{pre}}_{\mathrm{DG},i,t},P^{\mathrm{pre}}_{\mathrm{DG},j,t},\left(\sigma_{\mathrm{DG}}P^{\mathrm{pre}}_{\mathrm{DG},i,t}\right)^2,\left(\sigma_{\mathrm{DG}}P^{\mathrm{pre}}_{\mathrm{DG},i,t}\right)^2,\rho_{\mathrm{DG},ij,t}\right) \\ \tilde{Q}_{\mathrm{DG},i,t}=\dfrac{\tilde{P}_{\mathrm{DG},i,t}}{\tan\phi_{\mathrm{DG}}}\end{cases} \quad \forall i,\forall t \tag{5}$$

Coefficient $\rho_{\mathrm{DG},ij,t}$ reveals the correlation between DG outputs at bus i and bus j.

Rewriting (5) as matrix form, the active and reactive power of DG outputs during each period follows the N-dimensional multivariate Gaussian distributions in (6).

$$\begin{cases}\tilde{\boldsymbol{P}}_{\mathrm{DG},t}:\mathcal{N}_N\left(\boldsymbol{P}^{\mathrm{pre}}_{\mathrm{DG},t},\boldsymbol{\Sigma}^{\mathrm{DG}}_{t}\right)\\ \tilde{\boldsymbol{Q}}_{\mathrm{DG},t}:\mathcal{N}_N\left(\boldsymbol{K}_{\mathrm{DG}}\boldsymbol{P}^{\mathrm{pre}}_{\mathrm{DG},t},\boldsymbol{K}_{\mathrm{DG}}\boldsymbol{\Sigma}^{\mathrm{DG}}_{t}\boldsymbol{K}^{\mathrm{T}}_{\mathrm{DG}}\right)\end{cases} \quad \forall t \tag{6}$$

The explicit expressions of covariance matrix $\boldsymbol{\Sigma}^{\mathrm{DG}}_{t}$ and the coefficient matrix $\boldsymbol{K}_{\mathrm{DG}}$ in (6) are shown in Appendix A (A4) and (A5).

2) Deviation of Growth Prediction

The envelope-bound uncertainty method is also employed in the deviation of DG growth prediction as follows.

$$U_{\mathrm{DG}}\left(\alpha_{\mathrm{DG}},\varphi_{\mathrm{DG}}\right)=\left\{\varphi_{\mathrm{DG}}:\left|\varphi_{\mathrm{DG}}-1\right|\le\alpha_{\mathrm{DG}};\alpha_{\mathrm{DG}}\ge 0;\ \varphi_{\mathrm{DG}}\in\left[\left(1-\alpha_{\mathrm{DG}}\right),\left(1+\alpha_{\mathrm{DG}}\right)\right]\right\} \tag{7}$$

An envelope-bound uncertainty set, which is defined as information gap U_{DG}, is used to represent the uncertainty of DG integration capacity growth. The proportion of actuality to prediction φ_{DG}, which indicates the proportion of actuality to prediction in DGs, is a realization of U_{DG} and represents a future scenario of DG integration capacity growth. α_{DG} is the width of the information gap, which indicates the maximum deviation between the actuality and the prediction.

C. Active Management Measures

1) DR and Its Uncertainty

This paper mainly considers the incentive DR [27]. The operation constraints and cost of transferable load and reducible load are formulated.

Transferable load is a flexible DR mechanism [4], [28], which can be flexibly allocated within the allowable periods. There are several transferable loads in the industrial and commercial customers such as ice-storage systems and elec-

tric vehicle charging stations. Considering the potential of DR and power consumers' comfort, the operation constraints of transferable load are shown in (8)-(11).

$$\begin{cases} -\underline{\delta}_i^{\text{trans}} P_{\text{L},i,t}^{\text{pre}} \le P_{i,t}^{\text{trans}} \le \overline{\delta}_i^{\text{trans}} P_{\text{L},i,t}^{\text{pre}} \\ Q_{i,t}^{\text{trans}} = \left(Q_{\text{L},i,t}^{\text{pre}} / P_{\text{L},i,t}^{\text{pre}} \right) P_{i,t}^{\text{trans}} \end{cases} \quad \forall i, \forall t \tag{8}$$

$$\begin{cases} -y_i \underline{\delta}_{i,\min}^{\text{trans}} \le -\underline{\delta}_i^{\text{trans}} \le 0 \\ 0 \le \overline{\delta}_i^{\text{trans}} \le y_i \overline{\delta}_{i,\max}^{\text{trans}} \end{cases} \quad \forall i, \forall t \tag{9}$$

$$\sum_{i \in \Omega_{\text{bus}}} y_i \le N_{\max}^{\text{trans}} \tag{10}$$

$$\sum_{t \in \Omega_{\text{T}}} \left(P_{\text{L},i,t}^{\text{pre}} - P_{i,t}^{\text{trans}} \right) \Delta t = \sum_{t \in \Omega_{\text{T}}} P_{\text{L},i,t}^{\text{pre}} \Delta t \quad \forall i \tag{11}$$

If the transferring power $P_{i,t}^{\text{trans}}$ is greater than 0, the energy consumption is reduced. If $P_{i,t}^{\text{trans}}$ is smaller than 0, the energy consumption is increased. Constraint (8) ensures that $P_{i,t}^{\text{trans}}$ is within the adjusting range of transferable load. Constraint (9) denotes the decision of the transferring range, which is restricted by binary variable y_i (flag that allows this bus to implement load transferring) and the maximum transferring range $\left[\underline{\delta}_{i,\min}^{\text{trans}}, \overline{\delta}_{i,\max}^{\text{trans}} \right]$. Constraint (10) indicates the largest number of buses allowed to implement load transfer. Constraint (11) ensures that the sum of energy consumption after reductions and increases is equal to that of energy consumption without implementing DR, since the energy demand of transferable load (such as ice-storage system, electric vehicle charge) is constant.

The annual cost of DR includes incentive compensation and the cost of DR devices. The annual cost of transferable load in the bus i is shown as follows.

$$C_{\text{trans}} = \sum_{i \in \Omega_{\text{bus}}} \left(C_{\text{dev}}^{\text{trans}} \left(\overline{\delta}_i^{\text{trans}} + \underline{\delta}_i^{\text{trans}} \right) P_{\text{L},i}^{\text{pre,max}} + \sum_{\Omega_{\text{Y}}} C_{\text{price}}^{\text{trans}} \sum_{t \in \Omega_{\text{T}}} \left| P_{i,t}^{\text{trans}} \right| \right) \quad \forall i \tag{12}$$

Reducible loads include temperature control loads, building lighting loads, etc. Considering the potential of DR and power consumers' comfort, the operation constraints of reducible load are shown in (13)-(15).

$$\begin{cases} P_{i,t}^{\text{re}} \le \overline{\delta}_i^{\text{re}} P_{\text{L},i,t}^{\text{pre}} \\ Q_{i,t}^{\text{re}} = \dfrac{Q_{\text{L},i,t}^{\text{pre}}}{P_{\text{L},i,t}^{\text{pre}}} P_{i,t}^{\text{re}} \end{cases} \quad \forall i, \forall t \tag{13}$$

$$0 \le \overline{\delta}_i^{\text{re}} \le z_i \overline{\delta}_{i,\max}^{\text{re}} \quad \forall i, \forall t \tag{14}$$

$$\sum_{i \in \Omega_{\text{bus}}} z_i \le N_{\max}^{\text{re}} \tag{15}$$

Equation (13) ensures that $P_{i,t}^{\text{re}}$ is within the adjusting range of reducible load. Constraint (14) denotes the decision of the adjusting range, which is restricted by binary variable z_i (flag that allows this bus to implement load curtailment) and the maximum adjusting ratios $\overline{\delta}_{i,\max}^{\text{re}}$. Constraint (15) indicates the largest number of buses that are allowed to implement load reduction.

The annual cost of reducible load at bus i is shown as follows.

$$C_{\text{re}} = \sum_{i \in \Omega_{\text{bus}}} \left(C_{\text{dev}}^{\text{re}} \overline{\delta}_i^{\text{re}} P_{\text{L},i}^{\text{pre,max}} + \sum_{\Omega_{\text{Y}}} C_{\text{price}}^{\text{re}} \sum_{t \in \Omega_{\text{T}}} P_{i,t}^{\text{re}} \right) \quad \forall i \tag{16}$$

The implementation of DR depends on the willingness of customers, which implies uncertainty. This paper models the actual DR power as random variables following Gaussian distribution [29]. The variances change following the decision variables. Considering the correlation between response power in bus i and bus j, the stochastic characteristics of DR can be modeled as follows.

$$\begin{cases} \left(\tilde{P}_{i,t}^{\text{trans}}, \tilde{P}_{j,t}^{\text{trans}} \right): \\ \quad \mathcal{N}_{\text{bivariate}} \left(P_{i,t}^{\text{trans}}, P_{i,t}^{\text{trans}}, \left(\sigma_{\text{trans}} P_{i,t}^{\text{trans}} \right)^2, \left(\sigma_{\text{trans}} P_{j,t}^{\text{trans}} \right)^2, \rho_{\text{trans},ij,t} \right) \\ \left(\tilde{P}_{i,t}^{\text{re}}, \tilde{P}_{j,t}^{\text{re}} \right): \\ \quad \mathcal{N}_{\text{bivariate}} \left(P_{i,t}^{\text{re}}, P_{j,t}^{\text{re}}, \left(\sigma_{\text{re}} P_{i,t}^{\text{re}} \right)^2, \left(\sigma_{\text{re}} P_{j,t}^{\text{re}} \right)^2, \rho_{\text{re},ij,t} \right) \end{cases} \quad \forall i,j, \forall t \tag{17}$$

Rewriting (17) as matrix form, the active and reactive power of two kinds of DR during each period follow the N-dimensional multivariate Gaussian distributions in (18) and (19), respectively.

$$\begin{cases} \tilde{\boldsymbol{P}}_t^{\text{trans}} : \mathcal{N}_N \left(\boldsymbol{P}_t^{\text{trans}}, \boldsymbol{\Sigma}_t^{\text{trans}} \right) \\ \tilde{\boldsymbol{Q}}_t^{\text{trans}} : \mathcal{N}_N \left(\boldsymbol{K}_t^{\text{L}} \boldsymbol{P}_t^{\text{trans}}, \boldsymbol{K}_t^{\text{L}} \boldsymbol{\Sigma}_t^{\text{trans}} \boldsymbol{K}_t^{\text{L}} \right) \end{cases} \quad \forall t \tag{18}$$

$$\begin{cases} \tilde{\boldsymbol{P}}_t^{\text{re}} : \mathcal{N}_N \left(\boldsymbol{P}_t^{\text{re}}, \boldsymbol{\Sigma}_t^{\text{re}} \right) \\ \tilde{\boldsymbol{Q}}_t^{\text{re}} : \mathcal{N}_N \left(\boldsymbol{K}_{\text{L}} \boldsymbol{P}_t^{\text{re}}, \boldsymbol{K}_{\text{L}} \boldsymbol{\Sigma}_t^{\text{re}} \boldsymbol{K}_{\text{L}}^{\text{T}} \right) \end{cases} \quad \forall t \tag{19}$$

The expressions of covariance matrices $\boldsymbol{\Sigma}_t^{\text{trans}}$, $\boldsymbol{\Sigma}_t^{\text{re}}$, and coefficient matrix $\boldsymbol{K}_t^{\text{L}}$ are shown in Appendix A (A6)-(A8).

2) DG Curtailment and Its Uncertainty

The primary measure of supply-side management is DG curtailment. The peak of DG output can be curtailed to alleviate the burden of system operation.

$$\begin{cases} P_{i,t}^{\text{cur}} \le \overline{\delta}_i^{\text{cur}} P_{\text{DG},i,t}^{\text{pre}} \\ Q_{i,t}^{\text{cur}} = \left(Q_{\text{DG},i,t}^{\text{pre}} / P_{\text{DG},i,t}^{\text{pre}} \right) P_{i,t}^{\text{cur}} \end{cases} \quad \forall i, \forall t \tag{20}$$

$$0 \le \overline{\delta}_i^{\text{cur}} \le 1 \quad \forall i, \forall t \tag{21}$$

Equation (20) ensures that $P_{i,t}^{\text{cur}}$ is within the adjusting range. Constraint (21) indicates the decision of the adjusting range.

The annual cost of DG curtailment is shown as follows.

$$C_{\text{cur}} = \sum_{i \in \Omega_{\text{bus}}} \left(C_{\text{dev}}^{\text{cur}} \overline{\delta}_i^{\text{cur}} P_{\text{DG},i}^{\text{pre,max}} + \sum_{\Omega_{\text{Y}}} C_{\text{price}}^{\text{cur}} \sum_{t \in \Omega_{\text{T}}} P_{i,t}^{\text{cur}} \right) \quad \forall i \tag{22}$$

Assuming that the DG operators act independently and invoke the central limit theorem [29], we model the actual response of curtailment instructions as random variables that follow Gaussian distribution. The variances follow the change of decision variables. Considering the correlation between curtailed DG outputs at bus i and bus j, the stochastic characteristics of DG curtailment can be modeled as follows.

$\left(\tilde{P}_{i,t}^{\text{cur}}, \tilde{P}_{j,t}^{\text{cur}}\right)$:

$$\mathcal{N}_{\text{bivariate}}\left(P_{i,t}^{\text{cur}}, P_{j,t}^{\text{cur}}, \left(\sigma_{\text{cur}} P_{i,t}^{\text{cur}}\right)^2, \left(\sigma_{\text{cur}} P_{i,t}^{\text{cur}}\right)^2, \rho_{\text{cur},ij,t}\right) \quad \forall i,j,\forall t \tag{23}$$

Rewriting (23) in matrix form, the active power and reactive power of DG curtailment during each period follow the N-dimensional multivariate Gaussian distributions in (24).

$$\begin{cases} \tilde{\boldsymbol{P}}_t^{\text{cur}} : \mathcal{N}_N\left(\boldsymbol{P}_t^{\text{cur}}, \boldsymbol{\Sigma}_t^{\text{cur}}\right) \\ \tilde{\boldsymbol{Q}}_t^{\text{cur}} : \mathcal{N}_N\left(\boldsymbol{K}_{\text{DG}} \boldsymbol{P}_t^{\text{cur}}, \boldsymbol{K}_{\text{DG}} \boldsymbol{\Sigma}_t^{\text{cur}} \boldsymbol{K}_{\text{DG}}^{\text{T}}\right) \end{cases} \quad \forall t \tag{24}$$

The expression of the covariance matrix $\boldsymbol{\Sigma}_t^{\text{cur}}$ is shown in Appendix A (A9).

3) Reactive Power Compensation

In this paper, we use CBs to implement reactive power compensation [2]. The operation constraints about CBs are shown as follows.

$$Q_{i,t}^{\text{cb}} = \beta_{i,t}^{\text{cb}} Q_i^{\text{cb,unit}} \quad \forall i \in \Omega_{\text{cb}}, \forall t \tag{25}$$

$$\delta_{i,t}^{\text{cb,in}} + \delta_{i,t}^{\text{cb,de}} \le 1 \quad \forall i \in \Omega_{\text{cb}}, \forall t \tag{26}$$

$$\sum_{t \in \Omega_{\text{T}}} \left(\delta_{i,t}^{\text{cb,in}} + \delta_{i,t}^{\text{cb,de}}\right) \le N_i^{\text{cb,daily}} \quad \forall i \in \Omega_{\text{cb}} \tag{27}$$

$$\begin{cases} \beta_{i,t}^{\text{cb}} - \beta_{i,t-1}^{\text{cb}} \le \delta_{i,t}^{\text{cb,in}} N_i^{\text{cb,max}} - \delta_{i,t}^{\text{cb,de}} \\ \beta_{i,t}^{\text{cb}} - \beta_{i,t-1}^{\text{cb}} \ge \delta_{i,t}^{\text{cb,in}} - \delta_{i,t}^{\text{cb,de}} N_i^{\text{cb,max}} \end{cases} \quad \forall i \in \Omega_{\text{cb}}, \forall t \tag{28}$$

Equation (25) denotes the discrete reactive power of CB. Constraint (26) indicates that each CB cannot increase and decrease reactive power simultaneously. Constraint (27) ensures that the switching actions of each CB do not exceed the daily allowable number. Constraint (28) restricts the operation range of CB considering the maximum bank numbers.

The annual cost of CB action is shown as follows.

$$C_{\text{cb}} = \sum_{\Omega_{\text{Y}}} C_{\text{price}}^{\text{cb}} \sum_{t \in \Omega_{\text{T}}} \sum_{i \in \Omega_{\text{cb}}} \left(\delta_{i,t}^{\text{cb,in}} + \delta_{i,t}^{\text{cb,de}}\right) \tag{29}$$

4) Dynamic Network Reconfiguration

We focus on dynamic network reconfiguration based on RCS [12] to remove grid congestion in real time. The constraints of reconfiguration in the Distflow model are shown as follows.

$$\begin{cases} -\beta_{ij,t}^{\text{nr}} M_1 \le P_{ij,t} \le \beta_{ij,t}^{\text{nr}} M_1 \\ -\beta_{ij,t}^{\text{nr}} M_2 \le Q_{ij,t} \le \beta_{ij,t}^{\text{nr}} M_2 \\ 0 \le l_{ij,t} \le \beta_{ij,t}^{\text{nr}} M_3 \end{cases} \quad \forall ij \in \Omega_{\text{rcs}}, \forall t \tag{30}$$

$$\begin{cases} v_{j,t} \le M_4\left(1 - \beta_{ij,t}^{\text{nr}}\right) + v_{i,t} - 2\left(R_{ij} P_{ij,t} + X_{ij} Q_{ij,t}\right) + \left(R_{ij}^2 + X_{ij}^2\right) l_{ij,t} \\ v_{j,t} \ge -M_4\left(1 - \beta_{ij,t}^{\text{nr}}\right) + v_{i,t} - 2\left(R_{ij} P_{ij,t} + X_{ij} Q_{ij,t}\right) + \left(R_{ij}^2 + X_{ij}^2\right) l_{ij,t} \end{cases} \quad \forall ij \in \Omega_{\text{rcs}}, \forall t \tag{31}$$

$$\sum_{ij \in \Omega_{\text{rcs}}} \beta_{ij,t}^{\text{nr}} = N - 1 \quad \forall t \tag{32}$$

$$\beta_{ij,1}^{\text{nr}} = \beta_{ij,T}^{\text{nr}} \quad \forall ij \in \Omega_{\text{rcs}} \tag{33}$$

Constraint (30) restricts the branch power flow by the big-M method. Constraint (31) restricts voltages considering network reconfiguration. Equation (32) limits the action of RCSs. Equation (33) guarantees that the states of RCSs are consistent at the beginning and end of the typical day.

The annual cost of network reconfiguration is shown as follows.

$$C_{\text{nr}} = \sum_{\Omega_{\text{Y}}} C_{\text{price}}^{\text{nr}} \sum_{t \in \Omega_{\text{T}}} \sum_{ij \in \Omega_{\text{rcs}}} \left|\beta_{ij,t}^{\text{nr}} - \beta_{ij,t-1}^{\text{nr}}\right| \tag{34}$$

III. Active Management Decision Method Based on Chance-constrained IGD Model

In this section, an active management decision method is proposed. Firstly, a deterministic optimization model is proposed to obtain the optimal budget and active management strategy for the future scenario. Secondly, a chance-constrained IGD model is proposed to obtain the robust adaptability of multiple uncertainties.

A. Deterministic Optimization of Active Management Strategy

The DSO utilizes active management schemes to support the integration of DGs and loads with the minimum annual comprehensive cost F, which includes the annual cost of active management and the annual energy loss cost of the DN. The objective function is formed as follows.

$$\min F = C_{\text{trans}} + C_{\text{re}} + C_{\text{cur}} + C_{\text{cb}} + C_{\text{nr}} + C_{\text{loss}} \tag{35}$$

The costs of active management schemes are discussed in (12), (16), (22), (29), and (34). C_{loss} denotes the annual energy loss cost of the DN.

$$C_{\text{loss}} = \lambda_{\text{loss}} \sum_{N_{\text{Y}}} \sum_{t \in \Omega_{\text{T}}} \sum_{ij \in \Omega_{\text{branch}}} l_{ij,t} R_{ij} \Delta T \tag{36}$$

The constraints are discussed as follows.

1) Power flow constraints of the DN are shown as follows.

$$\begin{cases} \sum_{i \in end(j)} \left[P_{ij,t} - R_{ij} l_{ij,t}\right] = \sum_{k \in head(j)} \left(P_{jk,t} + P_{j,t}\right) \\ \sum_{i \in end(j)} \left[Q_{ij,t} - X_{ij} l_{ij,t}\right] = \sum_{k \in head(j)} \left(Q_{jk,t} + Q_{j,t}\right) \end{cases} \quad \forall j, \forall t \tag{37}$$

$$\begin{cases} P_{j,t} = P_{\text{L},i,t}^{\text{pre}} - P_{j,t}^{\text{trans}} - P_{j,t}^{\text{re}} - \left(P_{\text{DG},j,t} - P_{j,t}^{\text{cur}}\right) \\ Q_{j,t} = Q_{\text{L},i,t}^{\text{pre}} - Q_{j,t}^{\text{trans}} - Q_{j,t}^{\text{re}} - \left(Q_{\text{DG},j,t} - Q_{j,t}^{\text{cur}}\right) - Q_{i,t}^{\text{cb}} \end{cases} \quad \forall j, \forall t \tag{38}$$

$$v_{j,t} = v_{i,t} - 2\left(R_{ij} P_{ij,t} + X_{ij} Q_{ij,t}\right) + \left(R_{ij}^2 + X_{ij}^2\right) l_{ij,t} \quad \forall ij, \forall t \tag{39}$$

$$v_{i,t} l_{ij,t} = P_{ij,t}^2 + Q_{ij,t}^2 \quad \forall ij, \forall t \tag{40}$$

where $end(j)$ denotes the head buses of some branches, and the end of these branches are bus j. $head(j)$ denotes the end buses of some branches, and the head of these branches are bus j.

2) Constraints of active management include constraints (8)-(11), (13)-(15), (21), (22), (25)-(28), and (30)-(33).

3) Security constraints for the DN include bus voltage constraints, branch thermal constraints [30], and substation capacity constraints [26].

$$V_{\min}^2 \le v_{i,t} \le V_{\max}^2 \quad \forall i, \forall t \tag{41}$$

$$P_{ij,t}^2 + Q_{ij,t}^2 \le S_{ij,\max}^2 \quad \forall ij, \forall t \tag{42}$$

$$\left(P_{i,t}^{\text{SUB}}\right)^2 + \left(Q_{i,t}^{\text{SUB}}\right)^2 \le \left(S_{i,\max}^{\text{SUB}}\right)^2 \quad \forall i \in \Omega_{\text{SUB}}, \forall t \tag{43}$$

The decision variables of the deterministic model can be concluded as follows.

1) The decision variables related to transferable load are $\overline{\delta}_i^{\text{trans}}$, $\underline{\delta}_i^{\text{trans}}$, $P_{i,t}^{\text{trans}}$, and y_i.

2) The decision variables related to reducible load are $\overline{\delta}_i^{\text{re}}$, $P_{i,t}^{\text{re}}$, and $z_{i,t}$.

3) The decision variables related to DG curtailment are $\overline{\delta}_i^{\text{cur}}$ and $P_{i,t}^{\text{cur}}$.

4) The decision variables related to reactive power compensation are $\delta_{i,t}^{\text{cb, in}}$, $\delta_{i,t}^{\text{cb, de}}$, and $\beta_{i,t}^{\text{cb}}$.

5) The decision variable related to network reconfiguration is $\beta_{ij,t}^{\text{nr}}$.

B. Multi-objective Chance-constrained IGD Model for Active Management

A chance-constrained IGD model with random variables and information gaps is proposed based on the deterministic model. The uncertainties of power fluctuations and active management could be analyzed by chance constraints. The uncertain deviations of growth prediction are quantitatively measured by the IGD model.

In practical projects, DSO usually prefers to obtain active management schemes which adapt to the extreme scenario. Therefore, the IGD model in this paper is mathematically formulated in the robust function [17]. In this formulation, the information gaps U_{L} and U_{DG} indicate the robust adaptability of the uncertainties in loads and DGs. To obtain the maximum adaptability of growth uncertainties, the objective functions $\max \alpha_{\text{L}}$ and $\max \alpha_{\text{DG}}$ are set since they reveal the widths of information gaps. To analyze the mutually restricted relationship between $\max \alpha_{\text{L}}$ and $\max \alpha_{\text{DG}}$, we need to optimize them simultaneously and consider them as a multi-objective problem.

$$\max_{\boldsymbol{u}} \left\{\alpha_{\text{L}}, \alpha_{\text{DG}}\right\} \tag{44}$$

Besides the constraints in the deterministic model, a constraint with a max term (robust function) needs to be added in the IGD model [10], [21] as follows.

$$\max_{\varphi_{\text{L}}, \varphi_{\text{DG}}} F_{\text{AM}} \le (1+v) F_{\text{AM0}} \tag{45}$$

$$F_{\text{AM}} = E_{\text{p}}\left(C_{\text{trans}} + C_{\text{re}} + C_{\text{cur}} + C_{\text{cb}} + C_{\text{nr}}\right) \tag{46}$$

Formulating F_{AM} as the mathematical expectation $E_{\text{p}}(\cdot)$ is necessary because random variables are introduced into the model. F_{AM0} is the basic active management cost derived from the deterministic optimization in Section III-A in the basic predicted scenario.

Constraint (45) indicates that the robust function F_{AM} in the worst future scenarios φ_{L}, φ_{DG}, belonging to information gaps $U_{\text{L}}\left(\alpha_{\text{L}}, \varphi_{\text{L}}\right)$, $U_{\text{DG}}\left(\alpha_{\text{DG}}, \varphi_{\text{DG}}\right)$, is still less than the given budget. Therefore, information gaps U_{L}, U_{DG} under maximum α_{L}, α_{DG} are the assessment result of the maximum robust adaptability of growth uncertainties.

In this paper, we use active management schemes to improve the controllability and uncertainty adaptability of DNs. It is meaningful to increase the budget of active management schemes to assess the improvement of controllability and adaptability. The increased budget of power loss cannot improve the controllability and adaptability of DNs. Thus, we select active management cost F_{AM} without network power losses as the objective function in (45).

However, the IGD model needs a reference value for robust function in (45), which is usually obtained from the basic scenario (the center of information gaps) [10], [21]. We select F_{AM0} as the reference value in (45) because it is a reasonable active management budget derived from optimal economic scheduling in the basic predicted scenario.

Then, the impact of growth deviations and power fluctuations in the deterministic model is analyzed. Considering the realizations of growth deviations derived from the IGD model, the prediction value of DGs and loads should be multiplied by φ_L and φ_{DG}, which is shown as follows.

$$\begin{cases} \hat{P}_{\text{L},i,t}^{\text{pre}} = \varphi_{\text{L}} P_{\text{L},i,t}^{\text{pre}} \\ \hat{P}_{\text{L},i}^{\text{pre, max}} = \varphi_{\text{L}} P_{\text{L},i}^{\text{pre, max}} \\ \hat{P}_{\text{DG},i,t}^{\text{pre}} = \varphi_{\text{DG}} P_{\text{DG},i,t}^{\text{pre}} \\ \hat{P}_{\text{DG},i}^{\text{pre, max}} = \varphi_{\text{DG}} P_{\text{DG},i}^{\text{pre, max}} \end{cases} \quad \forall i, \forall t \tag{47}$$

Considering the influence of short-term power fluctuations corresponding to the realizations of growth deviations in loads and DGs, the injections (38) in matrix form are updated as:

$$\begin{cases} \tilde{\boldsymbol{P}}_t = \tilde{\boldsymbol{P}}_{\text{L},t} - \tilde{\boldsymbol{P}}_t^{\text{trans}} - \tilde{\boldsymbol{P}}_t^{\text{re}} - \left(\tilde{\boldsymbol{P}}_{\text{DG},t} - \tilde{\boldsymbol{P}}_t^{\text{cur}}\right) \\ \tilde{\boldsymbol{Q}}_t = \tilde{\boldsymbol{Q}}_{\text{L},t} - \tilde{\boldsymbol{Q}}_t^{\text{trans}} - \tilde{\boldsymbol{Q}}_t^{\text{re}} - \left(\tilde{\boldsymbol{Q}}_{\text{DG},t} - \tilde{\boldsymbol{Q}}_t^{\text{cur}}\right) - \boldsymbol{Q}_t^{\text{cb}} \end{cases} \quad \forall t \tag{48}$$

According to (47) and (48), the injections follow the $2N$-dimensional multivariate Gaussian distribution, which can be formulated as follows.

$$\begin{bmatrix} \tilde{\boldsymbol{P}}_t \\ \tilde{\boldsymbol{Q}}_t \end{bmatrix} : \mathcal{N}_{2N}\left(\begin{bmatrix} \boldsymbol{\mu}_{\text{P},t} \\ \boldsymbol{\mu}_{\text{Q},t} \end{bmatrix}, \begin{bmatrix} \boldsymbol{\Sigma}_{\text{P},t} & \boldsymbol{\Sigma}_{\text{PQ},t} \\ \boldsymbol{\Sigma}_{\text{QP},t} & \boldsymbol{\Sigma}_{\text{Q},t} \end{bmatrix}\right) \quad \forall t \tag{49}$$

Based on the information of related random variables in (3), (6), (18), (19), and (24), the expressions of the elements in (49) are shown in (50)-(52).

1) The elements related to active power are expressed as:

$$\begin{cases} \boldsymbol{\mu}_{\text{P},t} = \hat{\boldsymbol{P}}_{\text{L},t}^{\text{pre}} - \boldsymbol{P}_t^{\text{trans}} - \boldsymbol{P}_t^{\text{re}} - \hat{\boldsymbol{P}}_{\text{DG},t}^{\text{pre}} + \boldsymbol{P}_t^{\text{cur}} \\ \boldsymbol{\Sigma}_{\text{P},t} = \boldsymbol{\Sigma}_t^{\text{L,P}} + \boldsymbol{\Sigma}_t^{\text{trans}} + \boldsymbol{\Sigma}_t^{\text{re}} + \boldsymbol{\Sigma}_t^{\text{DG}} + \boldsymbol{\Sigma}_t^{\text{cur}} \end{cases} \quad \forall t \tag{50}$$

2) The elements related to reactive power are expressed as:

$$\begin{cases} \boldsymbol{\mu}_{\text{Q},t} = \hat{\boldsymbol{Q}}_{\text{L},t}^{\text{pre}} - \boldsymbol{K}_t^{\text{L}}\left(\boldsymbol{P}_t^{\text{trans}} + \boldsymbol{P}_t^{\text{re}}\right) - \boldsymbol{K}_t^{\text{DG}}\left(\hat{\boldsymbol{P}}_{\text{DG},t}^{\text{pre}} - \boldsymbol{P}_t^{\text{cur}}\right) - \boldsymbol{Q}_t^{\text{CB}} \\ \boldsymbol{\Sigma}_{\text{Q},t} = \boldsymbol{\Sigma}_t^{\text{L,Q}} + \boldsymbol{K}_t^{\text{L}}\left(\boldsymbol{\Sigma}_t^{\text{trans}} + \boldsymbol{\Sigma}_t^{\text{re}}\right)\left(\boldsymbol{K}_t^{\text{L}}\right)^{\text{T}} + \boldsymbol{K}_{\text{DG}}\left(\boldsymbol{\Sigma}_t^{\text{DG}} + \boldsymbol{\Sigma}_t^{\text{cur}}\right)\boldsymbol{K}_{\text{DG}}^{\text{T}} \end{cases} \quad \forall t \tag{51}$$

3) The correlations between active and reactive power injections are expressed as:

$$\begin{cases} \boldsymbol{\Sigma}_{\text{PQ},t} = \boldsymbol{\Sigma}_t^{\text{L,PQ}} + \left(\boldsymbol{\Sigma}_t^{\text{trans}} + \boldsymbol{\Sigma}_t^{\text{re}}\right)\boldsymbol{K}_t^{\text{L}} + \left(\boldsymbol{\Sigma}_t^{\text{DG}} + \boldsymbol{\Sigma}_t^{\text{cur}}\right)\boldsymbol{K}_t^{\text{DG}} \\ \boldsymbol{\Sigma}_{\text{PQ},t} = \boldsymbol{\Sigma}_{\text{QP},t} \end{cases} \quad \forall t \tag{52}$$

The deducing process of (52) is shown in Appendix A (A10).

Since the state variables have been transformed as random variables, it is necessary to rewrite the security constraints (41)-(43) as chance constraints, which reflect the restrictions on the probability of exceeding the limits.

$$\Pr\left\{V_{\min}^2 \le \tilde{v}_{i,t} \le V_{\max}^2\right\} \ge 1 - p_{\text{V}} \quad \forall i, \forall t \tag{53}$$

$$\Pr\left\{\tilde{P}_{ij,t}^2+\tilde{Q}_{ij,t}^2\le S_{ij,\max}^2\right\}\ge 1-p_{\mathrm{S}}\quad \forall ij,\forall t \tag{54}$$

$$\Pr\left\{\left(\tilde{P}_{i,t}^{\mathrm{SUB}}\right)^2+\left(\tilde{Q}_{i,t}^{\mathrm{SUB}}\right)^2\le\left(S_{i,\max}^{\mathrm{SUB}}\right)^2\right\}\ge 1-p_{\mathrm{SUB}}\quad \forall i\in\Omega_{\mathrm{SUB}},\forall t \tag{55}$$

where $\Pr\{\cdot\}$ is the probability that the inequality constraint holds.

Therefore, the constraints of the multi-objective chance-constrained IGD model include (4), (7)-(16), (20)-(22), (25)-(34), (37), (39), (40), (45)-(48), and (53)-(55).

The decision variables of the proposed model include α_{L}, α_{DG}, φ_{L}, φ_{DG}, and decision variables $\boldsymbol{u}$ of active management schemes in the deterministic model.

IV. Solving Method

This section proposes the solving method of the chance-constrained IGD model. Three crucial elements deserve attention, including the IGD model, the chance constraints, and the multi-objective programming. ① A systematic solving method of the max term constraint is proposed. ② The chance constraints are rewritten as linear constraints and SOC constraints, which transform the original model into the multi-objective mixed-integer second-order cone programming (MISOCP) model. ③ The ε constraint algorithm is used so that the result of the whole model can be obtained by a commercial solver directly. The specific introduction is as follows.

A. Transformation of IGD Model

To the best of the authors' knowledge, it is hard to tackle muti-objective programming with the max term constraints. The monotonic relationship between the deviations of growth prediction in loads and DGs and active management cost cannot be verified directly. Therefore, the max term transformation methods, which are proposed in [10], [17], [25], cannot achieve satisfying results in this paper. A systematic solving method based on linearized power flow and linear programming is proposed.

1) A Linearized Power Flow Model

A linearized power flow model for DNs [31] is introduced in this paper. The power flow equations considering multiple uncertainties for period t at all the buses can be expressed as follows.

$$\begin{bmatrix}\tilde{\boldsymbol{P}}_t\\ \tilde{\boldsymbol{Q}}_t\end{bmatrix}-\begin{bmatrix}\boldsymbol{B}_2^{\mathrm{col}}\\ -\boldsymbol{B}_1^{\mathrm{col}}\end{bmatrix}\theta_{1,t}-\begin{bmatrix}\boldsymbol{B}_1^{\mathrm{col}}\\ \boldsymbol{B}_2^{\mathrm{col}}\end{bmatrix}V_{1,t}=\begin{bmatrix}\boldsymbol{B}_2^{\mathrm{sub}} & \boldsymbol{B}_1^{\mathrm{sub}}\\ -\boldsymbol{B}_1^{\mathrm{sub}} & \boldsymbol{B}_2^{\mathrm{sub}}\end{bmatrix}\begin{bmatrix}\tilde{\boldsymbol{\theta}}_t\\ \tilde{\boldsymbol{V}}_t\end{bmatrix}\quad\forall t \tag{56}$$

$$\begin{cases}\boldsymbol{B}_1(i,j)=\dfrac{R_{ij}}{R_{ij}^2+X_{ij}^2} & i\ne j,\forall i,j\\ \boldsymbol{B}_2(i,j)=\dfrac{X_{ij}}{R_{ij}^2+X_{ij}^2} & i\ne j,\forall i,j\\ \boldsymbol{B}_1(i,i)=\displaystyle\sum_{ij\in\Omega_{\mathrm{branch}}}\frac{R_{ij}}{R_{ij}^2+X_{ij}^2} & \forall i,j\\ \boldsymbol{B}_2(i,i)=\displaystyle\sum_{ij\in\Omega_{\mathrm{branch}}}\frac{X_{ij}}{R_{ij}^2+X_{ij}^2} & \forall i,j\end{cases} \tag{57}$$

where $\boldsymbol{P}$, $\boldsymbol{Q}$, $\boldsymbol{\theta}$, and $\boldsymbol{V}$ are the vectors of active and reactive power injections, voltage angles, and voltage magnitudes, respectively, except the reference bus; $\boldsymbol{B}_1^{\mathrm{sub}}$ and $\boldsymbol{B}_2^{\mathrm{sub}}$ are the sub-matrices of $\boldsymbol{B}_1$ and $\boldsymbol{B}_2$ excluding the first row and the first column; $\boldsymbol{B}_1^{\mathrm{col}}$ and $\boldsymbol{B}_2^{\mathrm{col}}$ are the first columns in $\boldsymbol{B}_1$ and $\boldsymbol{B}_2$ without the first element, respectively; θ_1 is the voltage angle of the reference bus and is equal to 0; and V_1 is the voltage magnitude of the reference bus. In this paper, we focus on the voltage magnitudes.

By application of the linearized power flow model, the IGD model can be solved within the linear programming framework.

2) Solving Method of Max Term Constraint

Based on the fundamental theorem of linear programming [32], a linear objective function defined over a polygonal convex set attains a maximum (or minimum) value at an extreme point (vertex) of the set.

The optimization of robust function in (45) based on the linearized power flow model belongs to the linear programming described in the theorem. Therefore, constraint (45) can be replaced by four constraints (58) about extreme points $(\varphi_{\mathrm{L}}:1\pm\alpha_{\mathrm{L}},\varphi_{\mathrm{DG}}:1\pm\alpha_{\mathrm{DG}})$, i. e., $(1-\alpha_L,1-\alpha_{DG})$, $(1+\alpha_L,1-\alpha_{DG})$, $(1-\alpha_L,1+\alpha_{DG})$, and $(1+\alpha_L,1+\alpha_{DG})$. The maximum value of $F_{AM}(\varphi_L,\varphi_{DG})$ achieves at one extreme point, while the values at the other extreme points are less than the maximum value.

$$\begin{cases}F_{\mathrm{AM}}(\boldsymbol{u},\varphi_{\mathrm{L}}:1-\alpha_{\mathrm{L}},\varphi_{\mathrm{DG}}:1-\alpha_{\mathrm{DG}})\le(1+\rho)F_{\mathrm{AM0}}\\ F_{\mathrm{AM}}(\boldsymbol{u},\varphi_{\mathrm{L}}:1-\alpha_{\mathrm{L}},\varphi_{\mathrm{DG}}:1+\alpha_{\mathrm{DG}})\le(1+\rho)F_{\mathrm{AM0}}\\ F_{\mathrm{AM}}(\boldsymbol{u},\varphi_{\mathrm{L}}:1+\alpha_{\mathrm{L}},\varphi_{\mathrm{DG}}:1-\alpha_{\mathrm{DG}})\le(1+\rho)F_{\mathrm{AM0}}\\ F_{\mathrm{AM}}(\boldsymbol{u},\varphi_{\mathrm{L}}:1+\alpha_{\mathrm{L}},\varphi_{\mathrm{DG}}:1+\alpha_{\mathrm{DG}})\le(1+\rho)F_{\mathrm{AM0}}\end{cases} \tag{58}$$

B. Transformation of Chance Constraints

For simplification of chance constraints, the expression of voltages is calculated first. Linear equation (56) is rewritten as follows.

$$\begin{bmatrix}\tilde{\boldsymbol{\theta}}_t\\ \tilde{\boldsymbol{V}}_t\end{bmatrix}=\boldsymbol{D}\begin{bmatrix}\tilde{\boldsymbol{P}}_t\\ \tilde{\boldsymbol{Q}}_t\end{bmatrix}-\boldsymbol{D}\begin{bmatrix}\boldsymbol{B}_1^{\mathrm{col}}\theta_{1,t}\\ \boldsymbol{B}_2^{\mathrm{col}}V_{1,t}\end{bmatrix}\quad\forall t \tag{59}$$

$$\boldsymbol{D}=\begin{bmatrix}\boldsymbol{B}_2^{\mathrm{sub}} & \boldsymbol{B}_1^{\mathrm{sub}}\\ -\boldsymbol{B}_1^{\mathrm{sub}} & \boldsymbol{B}_2^{\mathrm{sub}}\end{bmatrix}^{-1} \tag{60}$$

According to the aforementioned stochastic model of the injections, the voltages $\tilde{\boldsymbol{V}}_t$ and $\tilde{\boldsymbol{\theta}}_t$ follow the multivariate Gaussian distribution as follows.

$$\begin{bmatrix}\tilde{\boldsymbol{\theta}}_t\\ \tilde{\boldsymbol{V}}_t\end{bmatrix}:\mathcal{N}_{2N}\left(\boldsymbol{D}\begin{bmatrix}\boldsymbol{\mu}_{\mathrm{P},t}\\ \boldsymbol{\mu}_{\mathrm{Q},t}\end{bmatrix}-\boldsymbol{D}\begin{bmatrix}\boldsymbol{B}_1^{\mathrm{col}}\theta_{1,t}\\ \boldsymbol{B}_2^{\mathrm{col}}V_{1,t}\end{bmatrix},\boldsymbol{D}\begin{bmatrix}\boldsymbol{\Sigma}_{\mathrm{P},t} & \boldsymbol{\Sigma}_{\mathrm{PQ},t}\\ \boldsymbol{\Sigma}_{\mathrm{QP},t} & \boldsymbol{\Sigma}_{\mathrm{Q},t}\end{bmatrix}\boldsymbol{D}^{\mathrm{T}}\right)\quad\forall t \tag{61}$$

The elements of the matrices in (61) have already been discussed in (50)-(52). For simplification, (45) can be summarized as follows.

$$\begin{bmatrix}\tilde{\boldsymbol{\theta}}_t\\ \tilde{\boldsymbol{V}}_t\end{bmatrix}:\mathcal{N}_{2N}\left(\begin{bmatrix}\boldsymbol{\mu}_{\theta,t}\\ \boldsymbol{\mu}_{\mathrm{V},t}\end{bmatrix},\begin{bmatrix}\boldsymbol{\Sigma}_{\theta,t} & \boldsymbol{\Sigma}_{\theta\mathrm{V},t}\\ \boldsymbol{\Sigma}_{\mathrm{V}\theta,t} & \boldsymbol{\Sigma}_{\mathrm{V},t}\end{bmatrix}\right)\quad\forall t \tag{62}$$

Based on the nature of normal distribution, the voltage amplitudes follow:

$$\tilde{\boldsymbol{V}}_t:\sqrt{\boldsymbol{\Sigma}_{\mathrm{V},t}}\,\boldsymbol{\Phi}+\boldsymbol{\mu}_{\mathrm{V},t}\quad\forall t \tag{63}$$

Then, the transformations of various security constraints are proposed as follows.

1) Transformation of Bus Voltage Constraints

The chance constraint (53) can be rewritten as two parts because there is little probability of breaking the constraint from both sides.

$$\begin{cases} \Pr\left\{\tilde{V}_{i,t} \le V_{\max}\right\} \ge 1-p_{\mathrm{V}} \\ \Pr\left\{\tilde{V}_{i,t} \le V_{\min}\right\} \le p_{\mathrm{V}} \end{cases} \quad \forall i, \forall t \tag{64}$$

Based on (63), chance constraints (64) can be transformed as:

$$\begin{cases} \mu_{\mathrm{V},i,t} + \Phi^{-1}\left(1-p_{\mathrm{V}}\right)\sqrt{\Sigma_{\mathrm{V},t}(i,i)} \le V_{\max} \\ \mu_{\mathrm{V},i,t} - \Phi^{-1}\left(p_{\mathrm{V}}\right)\sqrt{\Sigma_{\mathrm{V},t}(i,i)} \ge V_{\min} \end{cases} \quad \forall i, \forall t \tag{65}$$

where Φ^{-1} is the inverse function of a standardized Gaussian distribution. When p_{V} is smaller than 0.5, (65) can be transformed as linear constraints (66) and SOC constraints (67).

$$\begin{cases} \Phi^{-1}\left(1-p_{\mathrm{V}}\right)\lambda_{\mathrm{Vmax},i,t} = V_{\max} - \mu_{\mathrm{V},i,t} \\ \Phi^{-1}\left(1-p_{\mathrm{V}}\right)\lambda_{\mathrm{Vmin},i,t} = \mu_{\mathrm{V},i,t} - V_{\min} \end{cases} \quad \forall i, \forall t \tag{66}$$

$$\begin{cases} \lambda^2_{\mathrm{Vmax},i,t} \ge \Sigma_{\mathrm{V},t}(i,i) \\ \lambda^2_{\mathrm{Vmin},i,t} \ge \Sigma_{\mathrm{V},t}(i,i) \end{cases} \quad \forall i, \forall t \tag{67}$$

The squares of these auxiliary variables are greater than or equal to the variances of bus voltages $\Sigma_{\mathrm{V},t}(i,i)$. According to (62), $\Sigma_{\mathrm{V},t}(i,i)$ represents linear combinations of constants and squared decision variables in the model.

2) Transformation of Branch Thermal Constraints

In [30], the branch thermal constraints are effectively approximated by the circular constraint linearization method. We introduce this method to this paper, and the chance constraints (54) are reformulated as follows.

$$\begin{cases} \Pr\left\{-S_{ij,\max} \le \tilde{P}_{ij,t} \le S_{ij,\max}\right\} \ge 1-p_{\mathrm{S}} \\ \Pr\left\{-S_{ij,\max} \le \tilde{Q}_{ij,t} \le S_{ij,\max}\right\} \ge 1-p_{\mathrm{S}} \\ \Pr\left\{-\sqrt{2}\,S_{ij,\max} \le \tilde{P}_{ij,t} + \tilde{Q}_{ij,t} \le \sqrt{2}\,S_{ij,\max}\right\} \ge 1-p_{\mathrm{S}} \\ \Pr\left\{-\sqrt{2}\,S_{ij,\max} \le \tilde{P}_{ij,t} - \tilde{Q}_{ij,t} \le \sqrt{2}\,S_{ij,\max}\right\} \ge 1-p_{\mathrm{S}} \end{cases} \quad \forall ij, \forall t \tag{68}$$

In [31], the power flows through the power lines can be calculated as follows.

$$\begin{cases} \tilde{P}_{ij,t} = \dfrac{R_{ij}}{R_{ij}^2+X_{ij}^2}\left(\tilde{V}_{i,t}-\tilde{V}_{j,t}\right) + \dfrac{X_{ij}}{R_{ij}^2+X_{ij}^2}\left(\tilde{\theta}_{i,t}-\tilde{\theta}_{j,t}\right) \\ \tilde{Q}_{ij,t} = -\dfrac{R_{ij}}{R_{ij}^2+X_{ij}^2}\left(\tilde{\theta}_{i,t}-\tilde{\theta}_{j,t}\right) + \dfrac{X_{ij}}{R_{ij}^2+X_{ij}^2}\left(\tilde{V}_{i,t}-\tilde{V}_{j,t}\right) \end{cases} \quad \forall ij, \forall t \tag{69}$$

The difference in voltage amplitudes and the difference in voltage angles in (69) follow the bivariate Gaussian distribution (70), which can be derived from (71).

$$\left(V_{i,t}-V_{j,t}, \theta_{i,t}-\theta_{j,t}\right): \quad \mathcal{N}_{\mathrm{bivariate}}\left(E_{\mathrm{V},ij,t}, E_{\theta,ij,t}, D_{\mathrm{V},ij,t}, D_{\theta,ij,t}, \rho_{\mathrm{V}\theta,ij,t}\right) \quad \forall ij, \forall t \tag{70}$$

$$\rho_{\mathrm{V}\theta,ij,t} = \frac{Cov_{\mathrm{V}\theta,ij,t}}{\sqrt{D_{\mathrm{V},ij,t}}\sqrt{D_{\theta,ij,t}}} \tag{71}$$

The expressions of elements in (70) and (71) are shown in Appendix A (A11) and (A12). Based on (69) - (71), the branch power flows follow the distributions as follows.

$$\begin{cases} \tilde{P}_{ij,t}: \sigma_{\mathrm{P},ij,t}\Phi + \mu_{\mathrm{P},ij,t} \\ \tilde{Q}_{ij,t}: \sigma_{\mathrm{Q},ij,t}\Phi + \mu_{\mathrm{Q},ij,t} \\ \tilde{P}_{ij,t} + \tilde{Q}_{ij,t}: \sigma_{\mathrm{P+Q},ij,t}\Phi + \mu_{\mathrm{P+Q},ij,t} \\ \tilde{P}_{ij,t} - \tilde{Q}_{ij,t}: \sigma_{\mathrm{P-Q},ij,t}\Phi + \mu_{\mathrm{P-Q},ij,t} \end{cases} \quad \forall ij, \forall t \tag{72}$$

where σ_{P}, σ_{Q}, $\sigma_{\mathrm{P+Q}}$, and $\sigma_{\mathrm{P-Q}}$ donate the standard deviations of the corresponding random variables; and μ_{P}, μ_{Q}, $\mu_{\mathrm{P+Q}}$, and $\mu_{\mathrm{P-Q}}$ donate the expectations of the corresponding random variables. The expressions of aforementioned variables in (72) are shown in Appendix A. When p_{S} is smaller than 0.5, (68) can be transformed as linear constraints (73) and SOC constraints (74) based on the properties of (72).

$$\begin{cases} \Phi^{-1}\left(1-p_{\mathrm{S}}\right)\lambda_{\mathrm{Pmax},i,t} = S_{ij,\max} - \mu_{\mathrm{P},ij,t} \\ \Phi^{-1}\left(1-p_{\mathrm{S}}\right)\lambda_{\mathrm{Pmin},i,t} = \mu_{\mathrm{P},ij,t} + S_{ij,\max} \\ \Phi^{-1}\left(1-p_{\mathrm{S}}\right)\lambda_{\mathrm{Qmax},i,t} = S_{ij,\max} - \mu_{\mathrm{Q},ij,t} \\ \Phi^{-1}\left(1-p_{\mathrm{S}}\right)\lambda_{\mathrm{Qmin},i,t} = \mu_{\mathrm{Q},ij,t} + S_{ij,\max} \\ \Phi^{-1}\left(1-p_{\mathrm{S}}\right)\lambda_{\mathrm{P+Qmax},i,t} = \sqrt{2}\,S_{ij,\max} - \mu_{\mathrm{P+Q},ij,t} \\ \Phi^{-1}\left(1-p_{\mathrm{S}}\right)\lambda_{\mathrm{P+Qmin},i,t} = \mu_{\mathrm{P+Q},ij,t} + \sqrt{2}\,S_{ij,\max} \\ \Phi^{-1}\left(1-p_{\mathrm{S}}\right)\lambda_{\mathrm{P-Qmax},i,t} = \sqrt{2}\,S_{ij,\max} - \mu_{\mathrm{P-Q},ij,t} \\ \Phi^{-1}\left(1-p_{\mathrm{S}}\right)\lambda_{\mathrm{P-Qmin},i,t} = \mu_{\mathrm{P-Q},ij,t} + \sqrt{2}\,S_{ij,\max} \end{cases} \quad \forall i, \forall t \tag{73}$$

$$\begin{cases} \lambda^2_{\mathrm{Pmax},i,t} \ge \sigma^2_{\mathrm{P},ij,t} \\ \lambda^2_{\mathrm{Pmin},i,t} \ge \sigma^2_{\mathrm{P},ij,t} \\ \lambda^2_{\mathrm{Qmax},i,t} \ge \sigma^2_{\mathrm{Q},ij,t} \\ \lambda^2_{\mathrm{Qmin},i,t} \ge \sigma^2_{\mathrm{Q},ij,t} \\ \lambda^2_{\mathrm{P+Qmax},i,t} \ge \sigma^2_{\mathrm{P+Q},ij,t} \\ \lambda^2_{\mathrm{P+Qmin},i,t} \ge \sigma^2_{\mathrm{P+Q},ij,t} \\ \lambda^2_{\mathrm{P-Qmax},i,t} \ge \sigma^2_{\mathrm{P-Q},ij,t} \\ \lambda^2_{\mathrm{P-Qmin},i,t} \ge \sigma^2_{\mathrm{P-Q},ij,t} \end{cases} \quad \forall i, \forall t \tag{74}$$

The squares of these auxiliary variables are greater than or equal to the related variances. According to Appendix A (A13)-(A16), the variances represent linear combinations of constants and squared decision variables in the model.

3) Transformation of Substation Capacity Constraints

The substation capacity constraints limit the power injections at the substation bus. They limit the power flow of branches that connect to the substation bus. Therefore, the chance-constrained substation capacity constraints (55) can be reformulated as follows.

$$\Pr\left\{\left(\sum_{j\in end(i)}\tilde{P}_{ij,t}\right)^2 + \left(\sum_{j\in end(i)}\tilde{Q}_{ij,t}\right)^2 \le \left(S^{\mathrm{SUB}}_{i,\max}\right)^2\right\} \ge 1-p_{\mathrm{SUB}} \quad \forall i \in \Omega_{\mathrm{SUB}}, \forall t \tag{75}$$

Thus, the tackling method is similar to the transformation process of branch thermal constraints, which is discussed in Appendix A (A17).

C. Solving Procedure

Based on the mathematical method mentioned in Section IV-A and IV-B, the original chance-constrained IGD model is transformed into a multi-objective MISOCP model. ε-constraint method is a fast and effective method for solving multi-objective programming [33]. It can transform the multi-objective MISOCP into several single-objective optimization problems, and the Pareto front is obtained by iteration.

V. Case Study

In this section, a modified IEEE 33-bus DN [2] is chosen to validate the proposed model. The amount of load is 1.2 times as large as the original value to represent the growth prediction in the future. The network structure of the modified IEEE 33-bus DN is presented in Fig. 1. The broken lines indicate the RCSs in the open state. The available capacity of the substation is 6 MVA. The predicted DG penetration level (proportion of max power) is 75%. The power factor of DGs is set to be 0.95.

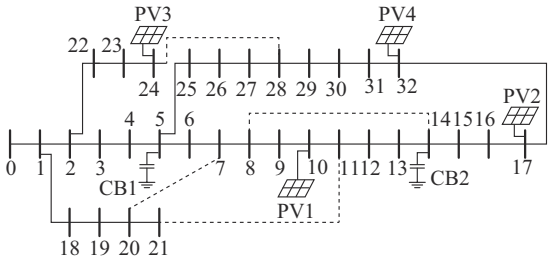

Fig. 1. Network structure of modified IEEE 33-bus DN.

Assuming that each load and DG can participate in active management and each branch has an RCS to implement reconfiguration. Considering the comfort of power consumers, the number of buses participating in DR cannot be more than half. The prices of DR and DG curtailment are from [4] and [5], respectively. The limitations of the transfer rate range from −30% ($\underline{\delta}^{\text{trans}}_{i,\min}$) to 30% ($\bar{\delta}^{\text{trans}}_{i,\max}$) and the limitation of the reduction rate is 20% ($\bar{\delta}^{\text{re}}_{i,\max}$). The prices of RCS and CB actions are from [2]. The step size of CBs is 0.05 Mvar, and there are 5 CBs in each CB bus. Confidence levels $1-p_{\text{V}}$, $1-p_{\text{S}}$, and $1-p_{\text{SUB}}$ of chance constraints are 0.95, which indicates that the probabilities of the security constraint holding are greater than 95%. The cost of active management reaches $1.5F_{\text{AM0}}$. For convenience, it is assumed that all coefficients of standard deviations are equal to 0.05. All correlation coefficients are set to be 0.5. The hourly variations of PV generation and load demands are obtained by prediction, which are shown in Fig. 2.

The simulation is carried out in MATLAB + YALMIP and commercial optimization solvers environment on an Intel-i5 computer with 3.1 GHz basic frequency and 16 GB RAM.

A. Simulation Results

The Pareto front for multi-objective function (44) in the basic scenario is presented as follows.

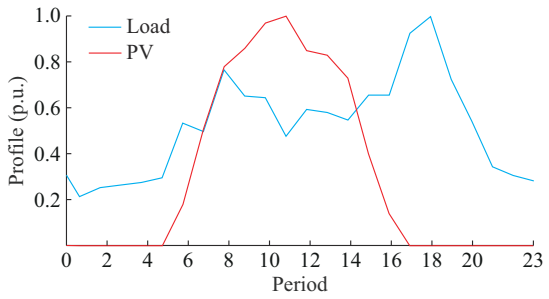

Fig. 2. Hourly variations of PV generation and load demands.

As shown in Fig. 3, when the active management cost is $1.5F_{\text{AM0}}$ (F_{AM0} is 177290 yuan (RMB), obtained from the deterministic model by SOCP), the black line presents the Pareto front formed by Pareto points from the ε-constraint method. The Pareto front includes a series of $(\alpha_{\text{L}}, \alpha_{\text{DG}})$ groups with the same active management cost and describes the boundaries of adaptable growth uncertainties in DGs and loads. Under the effect of active management schemes, the DN can accommodate DG capacity ranging from 26.7% to 173.3% (point P1 in Fig. 3) of prediction value at most. At this point, the DN cannot bear the deviations of the predicted load demand. Similarly, the DN can accommodate the loads ranging from 65.7% to 134.3% (point P3 in Fig. 3) of prediction value at most, while it is impossible to bear the deviations of predicted DG integration capacity.

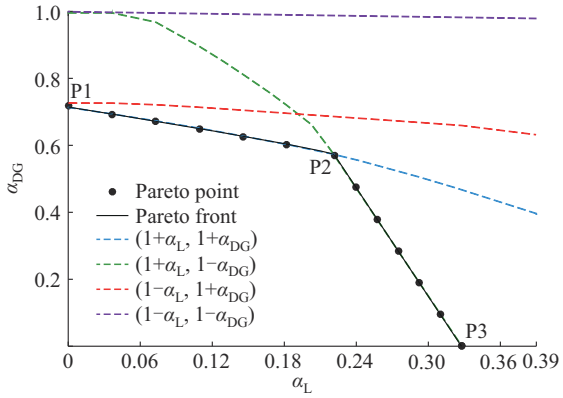

Fig. 3. Pareto front for (α_{L}, α_{DG}) and robust accommodation space Ω_{α}.

The active management schemes of DR and DG curtailment at the marked point P2 (0.222,0.576) are shown in Table II, and the schemes of reactive power compensation and network reconfiguration at P2 are shown in Figs. 4 and 5, respectively. In Fig. 5, the red lines indicate the closed RCSs during the specified period and the red broken lines indicate the opened section switches.

Two future scenarios in Fig. 3 are analyzed to verify the effectiveness of the proposed method in addressing security violation issues. The first scenario is at point P3, which is with 1.2 × 134.3% times the nominal values of loads in original IEEE 33-bus DN and 75% DG penetration level (referring to 1.2 times loads). Figure 6 shows the comparison of voltages at 18:00 with and without active management schemes at P3. The 90% confidence intervals (5% to 95%) of voltages at 18:00 are the lowest voltages during the day.

The active management schemes increase the voltages, and the voltage constraints hold with 95% probability.

TABLE II
ACTIVE MANAGEMENT SCHEME OF DR AND DG CURTAILMENT AT P2

Bus No.	y_i	$-\underline{\delta}_i^{\text{trans}}$ (%)	$\overline{\delta}_i^{\text{trans}}$ (%)	z_i	$\overline{\delta}_i^{\text{re}}$ (%)	$\overline{\delta}_i^{\text{CUR}}$ (%)
1	0			0		
2	0			0		
3	0			1	20.0	
4	0			0		
5	0			0		
6	0			0		
7	0			0		
8	0			0		
9	0			0		
10	0			0		29.85
11	1	−4.81	9.28	0		
12	0			0		
13	0			0		
14	0			0		
15	0			0		
16	0			0		
17	1	−30.00	30.00	1	20.0	26.94
18	0			0		
19	0			0		
20	0			0		
21	0			0		
22	0			0		
23	0			0		
24	1	−30.00	30.00	0		12.66
25	0			0		
26	0			0		
27	0			0		
28	0			0		
29	1	−27.10	30.00	0		
30	0			1	20.0	
31	0			1	20.0	
32	0			0		2.13

The second scenario is at point P1 in Fig. 3, which is with 1.2 times the nominal values of loads in the original IEEE 33-bus DN and 75% × 173.3% DG penetration level (referring to 1.2 times loads). Figure 7 shows the comparison of the voltages at 12:00 with and without active management schemes at P1. It shows 90% confidence intervals (5% to 95%) of voltages at 12:00, which are the highest voltages in the day. The active management schemes decrease the voltages, and voltage constraints hold with 95% probability.

The Pareto front and the coordinate axis of DGs and loads constitute the robust accommodation space Ω_α with growth deviation $(\alpha_{\text{L}}, \alpha_{\text{DG}})$. Furthermore, the Pareto front reveals a mutually restricted relationship between α_{DG} and α_{L}. This is because the expenditure is finite, and there exists a competition in improving the DG accommodation and load adaptability.

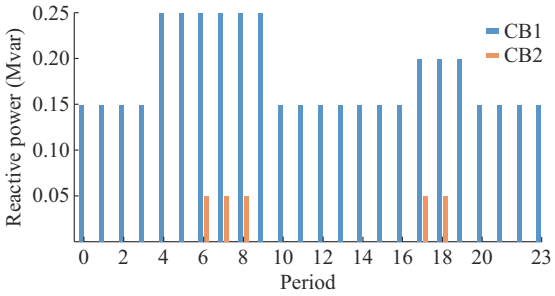

Fig. 4. Scheme of reactive power compensation at P2.

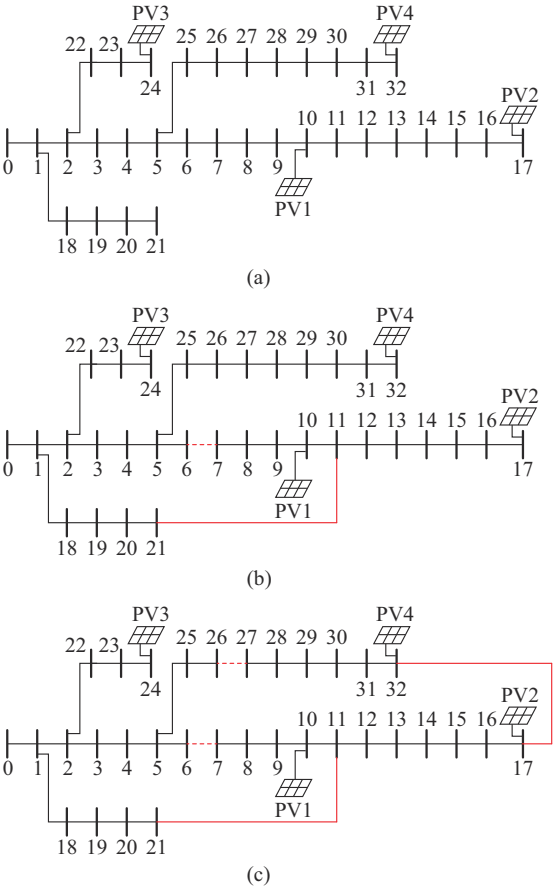

Fig. 5. Scheme of network reconfiguration at P2. (a) Configuration at 00:00-06:00 and 22:00-00:00. (b) Configuration at 06:00-10:00 and 16:00-22:00. (c) Configuration at 10:00-16:00.

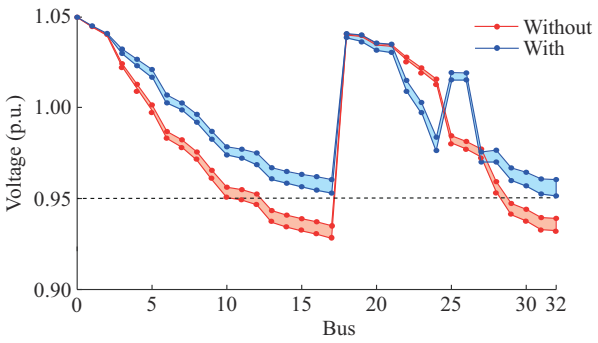

Fig. 6. Comparison of voltages at 18:00 with and without active management schemes at P3.

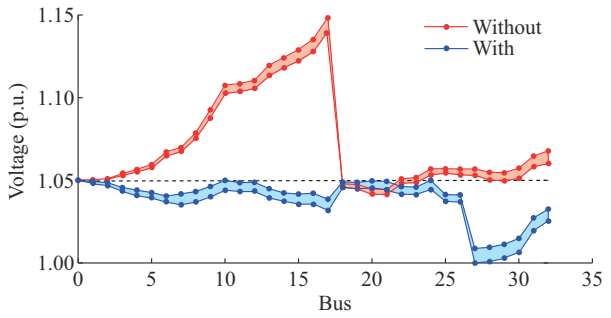

Fig. 7. Comparison of voltages at 12:00 with and without active management schemes at P1.

Note that each point (α_L, α_{DG}) on the Pareto front means that the corresponding active management scheme can burden four extreme scenarios $(1-\alpha_L, 1-\alpha_{DG})$, $(1+\alpha_L, 1-\alpha_{DG})$, $(1-\alpha_L, 1+\alpha_{DG})$, and $(1+\alpha_L, 1+\alpha_{DG})$, which are related to $(\varphi_L, \varphi_{DG})$ in this paper. Therefore, $\Omega_\alpha(\alpha_L, \alpha_{DG})$ can be extended into $\Omega_\varphi(\varphi_L, \varphi_{DG})$ to describe the adaptability of growth uncertainties more intuitively. The robust accommodation space Ω_φ of multiple uncertainties is shown in Fig. 8.

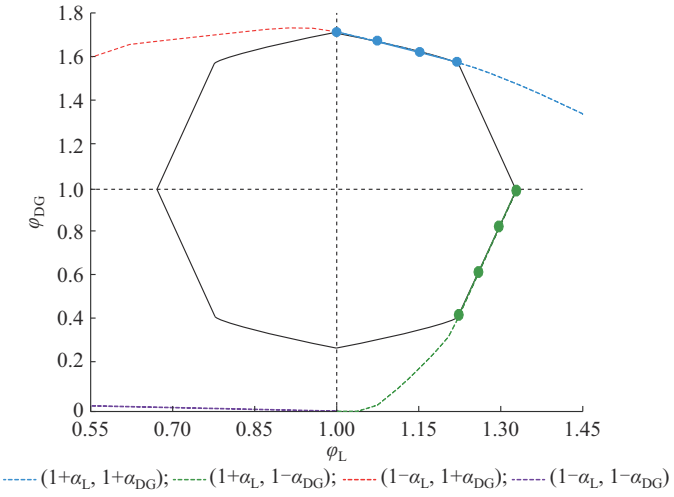

Fig. 8. Robust accommodation space Ω_φ of multiple uncertainties.

The black lines in Fig. 8 are the extended Pareto fronts and delineate the robust accommodation space Ω_φ. Every point $(\varphi_L, \varphi_{DG})$ within the robust accommodation space Ω_φ corresponds to a future scenario, and there can always be a related active management scheme with the cost equal to or less than the given budget value. Thus, the proposed method provides a "wait and see" active management strategy set instead of a "never be changed" planning scheme to confront the multiple uncertainties.

B. Effectiveness Analysis of Proposed Model

1) Validation for Characteristics of IGDT

The results illustrate the main characteristic of the IGD model. In the traditional optimization model (such as scenario-based stochastic programming and CCP), (α_L, α_{DG}) groups are inputs, and the active management cost is output. When enormous random (α_L, α_{DG}) groups are input, only a tiny part of them have the same cost as the given budget and become the points on the Pareto front, which is ineffective and confined. By contrast, the proposed model can systematically acquire the boundaries of adaptable growth uncertainties in DGs and loads. The comparison demonstrates that the proposed model is more appropriate for assessing the adaptability of uncertainties with limited cost.

2) Discussion on Pareto Front Form

The potential reasons for the Pareto front form are analyzed. Four inequations in (58) represent four possible extreme scenarios. When the model is solved another four times by involving every inequation of (58) in sequence, four Pareto fronts are plotted in Fig. 3 with different colors. Each Pareto front delineates the robust accommodation spaces of a corresponding possible extreme scenario. Constraint (58) demands that four inequalities hold at the same time. As a result, the robust accommodation space $\Omega_\alpha(\alpha_L, \alpha_{DG})$ is an intersection set of four original accommodation spaces. The final Pareto front may be a broken line constituted by different parts from four Pareto fronts because it is the boundary of the intersection set. Figure 3 indicates that the Pareto fronts of $(1+\alpha_L, 1+\alpha_{DG})$ and $(1+\alpha_L, 1-\alpha_{DG})$ form the final Pareto front.

In Fig. 8, four Pareto fronts are plotted in the four quadrants, respectively, with the same color series in Fig. 3. The worst scenario of four extreme scenarios can be analyzed by marking the corresponding boundaries. It is obvious that scenarios $(\varphi_L{:}1+\alpha_L, \varphi_{DG}{:}1+\alpha_{DG})$ and $(\varphi_L{:}1+\alpha_L, \varphi_{DG}{:}1-\alpha_{DG})$ are the worst scenarios and shape the robust accommodation space Ω_φ.

3) Comparison with Other IGDT Methods

The previous literature [10], [17], [25] transforms the max term in (45) by demonstrating the relationship between the objective function and decision variables. However, according to Fig. 3, we can find that the extreme scenario lies in $(1+\alpha_L, 1+\alpha_{DG})$ from P1 to P2 and $(1+\alpha_L, 1-\alpha_{DG})$ from P2 to P3, and it means that the max term has different expression in different parts of the Pareto front. This phenomenon cannot be analyzed in advance. Therefore, the previous methods cannot obtain the results shown in this paper, and the effectiveness of the proposed model is proven well.

4) Analysis of Worst Scenarios

In Fig. 3, the worst scenario about the deviation of DG growth shifts from $1+\alpha_{DG}$ to $1-\alpha_{DG}$ at P2. After analyzing this result in detail, we describe the cause as follows. ① When the positive deviation of load growth is slight, higher DG penetration levels tends to cause the overvoltage risk at noon, and $1+\alpha_{DG}$ can be the worst scenario which needs the highest cost to implement active management. ② When the positive deviation of load growth is quite large, under-voltage can be a main potential risk that requires more load reduction or transfer, and lower DG penetration level will decrease voltage so that $1-\alpha_{DG}$ becomes the worst scenario.

C. Sensitivity Analysis

1) Budgets for Active Management

The original F_{AM0} (v is equal to 0), which is the economic cost derived from the deterministic model, is input into the chance-constrained IGD model. However, the results show that the optimized α_{DG} and α_L are smaller than 0, and that

there is no Ω_φ available. It means the mere deterministic budget of active management cannot support future scenarios with multiple uncertainties. Besides growth uncertainties in DGs and loads, adding chance constraints demands more active management resources, which means more cost.

Then, the robust accommodation space Ω_φ is tested with varied budget $(1+v)F_{\text{AM0}}$, as shown in Fig. 9. When the cost decreases from $1.5F_{\text{AM0}}$ to $1.3F_{\text{AM0}}$, the maximum α_{DG} decreases from 0.733 to 0.401 and the maximum α_{L} decreases from 0.343 to 0.149. As a result, Ω_φ extends while the budget gradually rises. The worst scenarios with different budgets are also shown in Fig. 9 by marking points with the same color in Figs. 3 and 8.

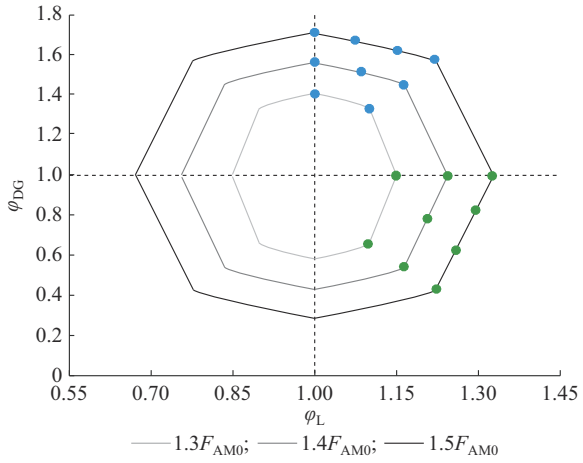

Fig. 9. Robust accommodation space Ω_φ with different budgets.

2) DG Penetration Level

By varying predicted DG penetration level from 75% to 125% and remaining other parameters constant, different accommodation spaces Ω_φ are obtained and illustrated as follows. In Fig. 10, when the predicted DG penetration level increases, the form of Ω_φ changes dynamically. The adaptability of DGs rapidly shrinks from 0.733 to 0.34 while α_{L} enlarges from 0.343 to 0.678. This situation can be explained as the rising DG penetration level provides the power supplement for load accommodation.

Note that a part of the worst scenarios at 125% penetration level is $(\varphi_{\text{L}}: 1-\alpha_{\text{L}}, \varphi_{\text{DG}}: 1+\alpha_{\text{DG}})$, which is different from other penetration conditions. When the DG power is higher than load demand, the power flow reverses, and over-voltage risk may appear in the daytime, and under-voltage may still happen at night. At 125% penetration level, the result indicates the accommodation ability in scenario $1-\alpha_{\text{L}}$ is less than the one in scenario $1+\alpha_{\text{L}}$, so that $1-\alpha_{\text{L}}$ is the more robust scenario.

3) Standard Deviations of Random Variables

The impact of power fluctuations is further discussed. The standard deviations of random variables vary from 0.05 to 0.1. The quantitative relationship between the robust accommodation space Ω_φ and different standard deviation coefficients is illustrated clearly in Fig. 11. Ω_φ becomes smaller (the maximum α_{DG} decreases from 0.733 to 0.336 and the maximum α_{L} decreases from 0.343 to 0.076) along with the enlargement of standard deviations.

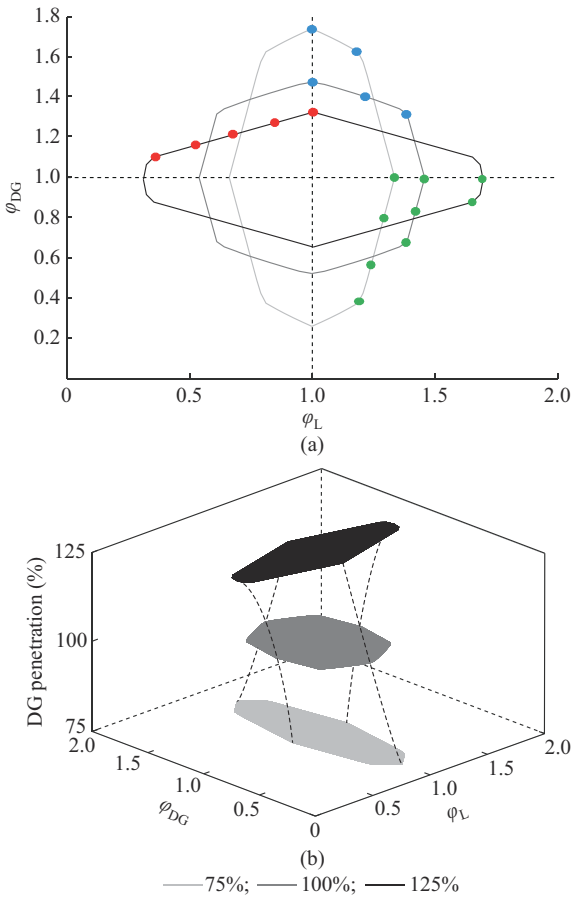

Fig. 10. Robust accommodation space Ω_φ with different DG penetration levels. (a) Robust accommodation space. (b) In 3-D plot.

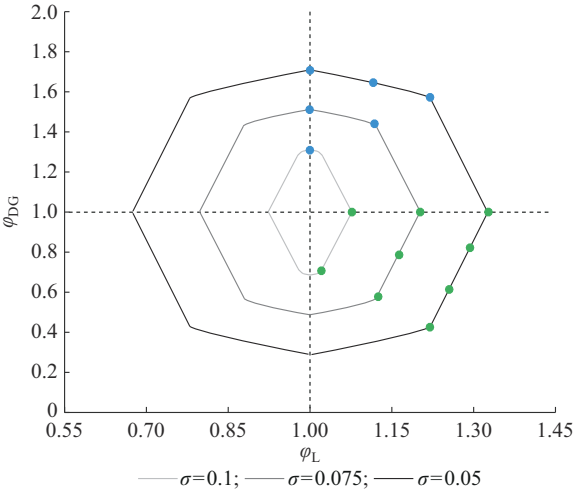

Fig. 11. Quantitative relationship between robust accommodation space Ω_φ and different standard deviation coefficients.

It indicates that the stochastic characteristic of power fluctuations and actual response (measured by standard deviation coefficients) negatively influences the adaptability of growth uncertainties in DGs and loads.

4) Correlation Coefficients of Random Variables

To test the impact of correlations, the correlation coefficients of random variables vary from 0.3 to 0.7. The quantitative relationship between the robust accommodation space

Ω_φ and correlation coefficients is illustrated clearly in Fig. 12. Ω_φ becomes smaller (the maximum α_{DG} decreases from 0.373 to 0.261 and the maximum α_L decreases from 0.811 to 0.628) along with the increase of correlation coefficients. It demonstrates that voltage fluctuations are stronger in a higher correlation coefficient scenario, which results in a smaller robust accommodation space.

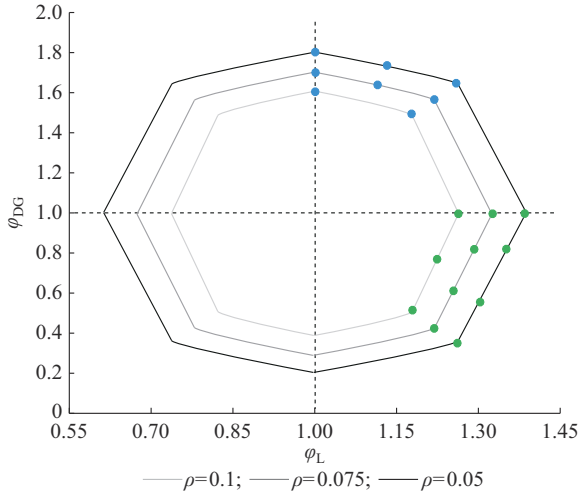

Fig. 12. Quantitative relationship between robust accommodation space Ω_φ and different standard correlation coefficients.

VI. Conclusion

In this paper, a scheduling method based on a multi-objective chance-constrained IGD model is proposed to obtain active management schemes for DSOs to address the security violation problem in various future scenarios. The maximum robust adaptability of multiple uncertainties, including the deviations of growth prediction and their relevant power fluctuations, can be obtained based on the limited budget of active management. A systematic solution method is proposed to reformulate the original model into a multi-objective MISOCP model by transforming the IGD model and chance constraints.

The simulation result delineates a robust accommodation space Ω_φ to represent the adaptability of multiple uncertainties. Every point $(\varphi_L, \varphi_{DG})$ within Ω_φ represents a future scenario, and there can always be a related active management scheme under the given budget. It demonstrates that the proposed method provides an optional active management strategy set to confront multiple uncertainties. The sensitivity analysis indicates that budget has a positive influence on the range of Ω_φ while standard deviation coefficients and correlation coefficients have the opposite impact.

In the future, we will focus on the diverse growth uncertainties at different buses and data-driven distributions for random variables to propose a more practical model.

Appendix A

A. Expressions of Covariance Matrices and Coefficient Matrices

The explicit expressions of the mentioned covariance matrices and coefficient matrices in Section II are given as follows.

$$\boldsymbol{\Sigma}_t^{L,P}=\begin{bmatrix} \left(\sigma_L^P P_{L,1,t}^{pre}\right)^2 & \rho_{L,(1,2),t}^P\left(\sigma_L^P\right)^2 P_{L,1,t}^{pre}P_{L,2,t}^{pre} & \cdots & \rho_{L,(1,N),t}^P\left(\sigma_L^P\right)^2 P_{L,1,t}^{pre}P_{L,N,t}^{pre} \\ \rho_{L,(2,1),t}^P\left(\sigma_L^P\right)^2 P_{L,2,t}^{pre}P_{L,1,t}^{pre} & \left(\sigma_L^P P_{L,2,t}^{pre}\right)^2 & \cdots & \rho_{L,(2,N),t}^P\left(\sigma_L^P\right)^2 P_{L,2,t}^{pre}P_{L,N,t}^{pre} \\ \vdots & \vdots & & \vdots \\ \rho_{L,(N,1),t}^P\left(\sigma_L^P\right)^2 P_{L,N,t}^{pre}P_{L,1,t}^{pre} & \rho_{L,(N,2),t}^P\left(\sigma_L^P\right)^2 P_{L,N,t}^{pre}P_{L,2,t}^{pre} & \cdots & \left(\sigma_L^P P_{L,N,t}^{pre}\right)^2 \end{bmatrix} \tag{A1}$$

$$\boldsymbol{\Sigma}_t^{L,Q}=\begin{bmatrix} \left(\sigma_L^Q Q_{L,1,t}^{pre}\right)^2 & \rho_{L,(1,2),t}^Q\left(\sigma_L^Q\right)^2 Q_{L,1,t}^{pre}Q_{L,2,t}^{pre} & \cdots & \rho_{L,(1,N),t}^Q\left(\sigma_L^Q\right)^2 Q_{L,1,t}^{pre}Q_{L,N,t}^{pre} \\ \rho_{L,(2,1),t}^Q\left(\sigma_L^Q\right)^2 Q_{L,2,t}^{pre}Q_{L,1,t}^{pre} & \left(\sigma_L^Q Q_{L,2,t}^{pre}\right)^2 & \cdots & \rho_{L,(2,N),t}^Q\left(\sigma_L^Q\right)^2 Q_{L,2,t}^{pre}Q_{L,N,t}^{pre} \\ \vdots & \vdots & & \vdots \\ \rho_{L,(N,1),t}^Q\left(\sigma_L^Q\right)^2 Q_{L,N,t}^{pre}Q_{L,1,t}^{pre} & \rho_{L,(N,2),t}^Q\left(\sigma_L^Q\right)^2 Q_{L,N,t}^{pre}Q_{L,2,t}^{pre} & \cdots & \left(\sigma_L^Q Q_{L,N,t}^{pre}\right)^2 \end{bmatrix} \tag{A2}$$

$$\boldsymbol{\Sigma}_t^{L,PQ}=\begin{bmatrix} \rho_{L,1,t}^{PQ}\left(\sigma_L^P P_{L,1,t}^{pre}\right)\left(\sigma_L^Q Q_{L,1,t}^{pre}\right) & 0 & \cdots & 0 \\ 0 & \rho_{L,2,t}^{PQ}\left(\sigma_L^P P_{L,2,t}^{pre}\right)\left(\sigma_L^Q Q_{L,2,t}^{pre}\right) & \cdots & 0 \\ \vdots & \vdots & & \vdots \\ 0 & 0 & \cdots & \rho_{L,N,t}^{PQ}\left(\sigma_L^P P_{L,N,t}^{pre}\right)\left(\sigma_L^Q Q_{L,N,t}^{pre}\right) \end{bmatrix} \tag{A3}$$

$$\boldsymbol{\Sigma}_t^{DG}=\begin{bmatrix} \left(\sigma_{DG} P_{DG,1,t}^{pre}\right)^2 & \rho_{DG,(1,2),t}\sigma_{DG}^2 P_{DG,1,t}^{pre}P_{DG,2,t}^{pre} & \cdots & \rho_{DG,(1,N),t}\sigma_{DG}^2 P_{DG,1,t}^{pre}P_{DG,N,t}^{pre} \\ \rho_{DG,(2,1),t}\sigma_{DG}^2 P_{DG,2,t}^{pre}P_{DG,1,t}^{pre} & \left(\sigma_{DG} P_{DG,2,t}^{pre}\right)^2 & \cdots & \rho_{L,(2,N),t}\sigma_{DG}^2 P_{DG,2,t}^{pre}P_{DG,N,t}^{pre} \\ \vdots & \vdots & & \vdots \\ \rho_{DG,(N,1),t}\sigma_{DG}^2 P_{DG,N,t}^{pre}P_{DG,1,t}^{pre} & \rho_{DG,(N,2),t}\sigma_{DG}^2 P_{DG,N,t}^{pre}P_{DG,2,t}^{pre} & \cdots & \left(\sigma_{DG} P_{DG,N,t}^{pre}\right)^2 \end{bmatrix} \tag{A4}$$

$$\boldsymbol{K}_{\mathrm{DG}}=\mathrm{diag}\left(\tan^{-1}\varphi_{\mathrm{DG}}\right)_{N\times N} \tag{A5}$$

$$\boldsymbol{K}_t^{\mathrm{L}}=\begin{bmatrix} Q_{\mathrm{L},1,t}^{\mathrm{pre}}/P_{\mathrm{L},1,t}^{\mathrm{pre}} & 0 & \cdots & 0 \\ 0 & Q_{\mathrm{L},2,t}^{\mathrm{pre}}/P_{\mathrm{L},2,t}^{\mathrm{pre}} & \cdots & 0 \\ \vdots & \vdots & & \vdots \\ 0 & 0 & \cdots & Q_{\mathrm{L},N,t}^{\mathrm{pre}}/P_{\mathrm{L},N,t}^{\mathrm{pre}} \end{bmatrix} \tag{A6}$$

$$\boldsymbol{\Sigma}_t^{\mathrm{trans}}=\begin{bmatrix} \left(\sigma_{\mathrm{trans}}P_{1,t}^{\mathrm{trans}}\right)^2 & \rho_{\mathrm{trans},(N,1),t}\sigma_{\mathrm{trans}}^2P_{1,t}^{\mathrm{trans}}P_{2,t}^{\mathrm{trans}} & \cdots & \rho_{\mathrm{trans},(1,N),t}\sigma_{\mathrm{trans}}^2P_{1,t}^{\mathrm{trans}}P_{N,t}^{\mathrm{trans}} \\ \rho_{\mathrm{trans},(2,1),t}\sigma_{\mathrm{trans}}^2P_{2,t}^{\mathrm{trans}}P_{1,t}^{\mathrm{trans}} & \left(\sigma_{\mathrm{trans}}P_{2,t}^{\mathrm{trans}}\right)^2 & \cdots & \rho_{\mathrm{trans},(2,N),t}\sigma_{\mathrm{trans}}^2P_{2,t}^{\mathrm{trans}}P_{N,t}^{\mathrm{trans}} \\ \vdots & \vdots & & \vdots \\ \rho_{\mathrm{trans},(N,1),t}\sigma_{\mathrm{trans}}^2P_{N,t}^{\mathrm{trans}}P_{1,t}^{\mathrm{trans}} & \rho_{\mathrm{trans},(N,2),t}\sigma_{\mathrm{trans}}^2P_{N,t}^{\mathrm{trans}}P_{2,t}^{\mathrm{trans}} & \cdots & \left(\sigma_{\mathrm{trans}}P_{N,t}^{\mathrm{trans}}\right)^2 \end{bmatrix} \tag{A7}$$

$$\boldsymbol{\Sigma}_t^{\mathrm{re}}=\begin{bmatrix} \left(\sigma_{\mathrm{re}}P_{1,t}^{\mathrm{re}}\right)^2 & \rho_{\mathrm{re},(N,1),t}\sigma_{\mathrm{re}}^2P_{1,t}^{\mathrm{re}}P_{2,t}^{\mathrm{re}} & \cdots & \rho_{\mathrm{re},(1,N),t}\sigma_{\mathrm{re}}^2P_{1,t}^{\mathrm{re}}P_{N,t}^{\mathrm{re}} \\ \rho_{\mathrm{re},(2,1),t}\sigma_{\mathrm{re}}^2P_{2,t}^{\mathrm{re}}P_{1,t}^{\mathrm{re}} & \left(\sigma_{\mathrm{re}}P_{2,t}^{\mathrm{re}}\right)^2 & \cdots & \rho_{\mathrm{re},(2,N),t}\sigma_{\mathrm{re}}^2P_{2,t}^{\mathrm{re}}P_{N,t}^{\mathrm{re}} \\ \vdots & \vdots & & \vdots \\ \rho_{\mathrm{re},(N,1),t}\sigma_{\mathrm{re}}^2P_{N,t}^{\mathrm{re}}P_{1,t}^{\mathrm{re}} & \rho_{\mathrm{re},(N,2),t}\sigma_{\mathrm{re}}^2P_{N,t}^{\mathrm{re}}P_{2,t}^{\mathrm{re}} & \cdots & \left(\sigma_{\mathrm{re}}P_{N,t}^{\mathrm{re}}\right)^2 \end{bmatrix} \tag{A8}$$

$$\boldsymbol{\Sigma}_t^{\mathrm{cur}}=\begin{bmatrix} \left(\sigma_{\mathrm{cur}}P_{1,t}^{\mathrm{cur}}\right)^2 & \rho_{\mathrm{cur},(N,1),t}\sigma_{\mathrm{cur}}^2P_{1,t}^{\mathrm{cur}}P_{2,t}^{\mathrm{cur}} & \cdots & \rho_{\mathrm{cur},(1,N),t}\sigma_{\mathrm{cur}}^2P_{1,t}^{\mathrm{cur}}P_{N,t}^{\mathrm{cur}} \\ \rho_{\mathrm{cur},(2,1),t}\sigma_{\mathrm{cur}}^2P_{2,t}^{\mathrm{cur}}P_{1,t}^{\mathrm{cur}} & \left(\sigma_{\mathrm{cur}}P_{2,t}^{\mathrm{cur}}\right)^2 & \cdots & \rho_{\mathrm{cur},(2,N),t}\sigma_{\mathrm{cur}}^2P_{2,t}^{\mathrm{cur}}P_{N,t}^{\mathrm{cur}} \\ \vdots & \vdots & & \vdots \\ \rho_{\mathrm{cur},(N,1),t}\sigma_{\mathrm{cur}}^2P_{N,t}^{\mathrm{cur}}P_{1,t}^{\mathrm{cur}} & \rho_{\mathrm{cur},(N,2),t}\sigma_{\mathrm{cur}}^2P_{N,t}^{\mathrm{cur}}P_{2,t}^{\mathrm{cur}} & \cdots & \left(\sigma_{\mathrm{cur}}P_{N,t}^{\mathrm{cur}}\right)^2 \end{bmatrix} \tag{A9}$$

B. Deducing Process of Covariance Matrix About Injections

The expression of covariance matrix $\boldsymbol{\Sigma}_{\mathrm{PQ},t}$ is deduced by the following process. The covariance between the active power injection of bus i and reactive power injection of bus j can be calculated as follows.

$$\begin{aligned} &Cov\left(\tilde{P}_{i,t},\tilde{Q}_{j,t}\right)=Cov\left(\tilde{P}_{\mathrm{L},i,t}-\tilde{P}_{i,t}^{\mathrm{trans}}-\tilde{P}_{i,t}^{\mathrm{re}}-\tilde{P}_{\mathrm{DG},i,t}+\tilde{P}_{i,t}^{\mathrm{cur}},\right. \\ &\left.\tilde{Q}_{\mathrm{L},i,t}-\tilde{Q}_{j,t}^{\mathrm{trans}}-\tilde{Q}_{j,t}^{\mathrm{re}}-\tilde{Q}_{\mathrm{DG},j,t}+\tilde{Q}_{j,t}^{\mathrm{cur}}-Q_{i,t}^{\mathrm{CB}}\right)= \\ &Cov\left(\tilde{P}_{\mathrm{L},i,t},\tilde{Q}_{\mathrm{L},i,t}\right)+Cov\left(\tilde{P}_{i,t}^{\mathrm{trans}},\tilde{Q}_{j,t}^{\mathrm{trans}}\right)+Cov\left(\tilde{P}_{i,t}^{\mathrm{re}},\tilde{Q}_{j,t}^{\mathrm{re}}\right)+ \\ &Cov\left(\tilde{P}_{\mathrm{DG},i,t},\tilde{Q}_{\mathrm{DG},j,t}\right)+Cov\left(\tilde{P}_{i,t}^{\mathrm{cur}},\tilde{Q}_{j,t}^{\mathrm{cur}}\right)= \\ &Cov\left(\tilde{P}_{\mathrm{L},i,t},\tilde{Q}_{\mathrm{L},i,t}\right)+Cov\left(\tilde{P}_{i,t}^{\mathrm{trans}},\boldsymbol{K}_t^{\mathrm{L}}(j,j)\tilde{P}_{j,t}^{\mathrm{trans}}\right)+ \\ &Cov\left(\tilde{P}_{i,t}^{\mathrm{re}},\boldsymbol{K}_t^{\mathrm{L}}(j,j)\tilde{P}_{j,t}^{\mathrm{re}}\right)+Cov\left(\tilde{P}_{\mathrm{DG},i,t},\boldsymbol{K}_{\mathrm{DG}}(j,j)\tilde{Q}_{\mathrm{DG},j,t}\right)+ \\ &Cov\left(\tilde{P}_{i,t}^{\mathrm{cur}},\boldsymbol{K}_{\mathrm{DG}}(j,j)\tilde{P}_{j,t}^{\mathrm{cur}}\right) \end{aligned} \tag{A10}$$

The summary of this expression in matrix form is shown in (52).

C. Details of Transformation of Chance Constraints About Branch Thermal Constraints.

The elements in (70) are shown in (A11).

$$\begin{cases} E_{\mathrm{V},ij,t}=\mu_{\mathrm{V},i,t}-\mu_{\mathrm{V},j,t} \\ D_{\mathrm{V},ij,t}=\sigma_{\mathrm{V},i,t}^2+\sigma_{\mathrm{V},j,t}^2+2\sigma_{\mathrm{V},ij,t}^2 \\ E_{\theta,ij,t}=\mu_{\theta,i,t}-\mu_{\theta,j,t} \\ D_{\theta,ij,t}=\sigma_{\theta,i,t}^2+\sigma_{\theta,j,t}^2+2\sigma_{\theta,ij,t}^2 \end{cases} \tag{A11}$$

The mentioned variables and parameters in (70) are shown in (A12).

$$\begin{aligned} &Cov_{\mathrm{V}\theta,ij,t}=Cov\left(V_{i,t}-V_{j,t},\theta_{i,t}-\theta_{j,t}\right)= \\ &\quad Cov\left(V_{i,t},\theta_{i,t}\right)+Cov\left(V_{j,t},\theta_{i,t}\right)+Cov\left(V_{i,t},\theta_{j,t}\right)+ \\ &\quad Cov\left(V_{j,t},\theta_{j,t}\right)=\sigma_{\mathrm{V}\theta,(i,i),t}^2+\sigma_{\mathrm{V}\theta,(j,j),t}^2+2\sigma_{\mathrm{V}\theta,(i,j),t}^2 \end{aligned} \tag{A12}$$

The mentioned variables and parameters in (72) are shown in (A13)-(A16).

$$\begin{cases} \sigma_{\mathrm{P},ij,t}=\dfrac{\sqrt{R_{ij}^2D_{\mathrm{V},ij,t}+X_{ij}^2D_{\theta,ij,t}+2R_{ij}X_{ij}Cov_{\mathrm{V}\theta,ij,t}}}{R_{ij}^2+X_{ij}^2} \\ \mu_{\mathrm{P},ij,t}=\dfrac{1}{R_{ij}^2+X_{ij}^2}\left(R_{ij}E_{\mathrm{V},ij,t}+X_{ij}E_{\theta,ij,t}\right) \end{cases} \tag{A13}$$

$$\begin{cases} \sigma_{\mathrm{Q},ij,t}=\dfrac{\sqrt{X_{ij}^2D_{\mathrm{V},ij,t}+R_{ij}^2D_{\theta,ij,t}+2R_{ij}X_{ij}Cov_{\mathrm{V}\theta,ij,t}}}{R_{ij}^2+X_{ij}^2} \\ \mu_{\mathrm{Q},ij,t}=\dfrac{X_{ij}E_{\mathrm{V},ij,t}+R_{ij}E_{\theta,ij,t}}{R_{ij}^2+X_{ij}^2} \end{cases} \tag{A14}$$

$$\begin{cases} \sigma_{\mathrm{P+Q},ij,t} = \dfrac{1}{R_{ij}^2+X_{ij}^2}\sqrt{\left(R_{ij}+X_{ij}\right)^2 D_{\mathrm{V},ij,t} + \left(X_{ij}-R_{ij}\right)^2 D_{\theta,ij,t} + 2\left(R_{ij}+X_{ij}\right)\left(X_{ij}-R_{ij}\right)Cov_{\mathrm{V}\theta,ij,t}} \\ \mu_{\mathrm{P+Q},ij,t} = \dfrac{1}{R_{ij}^2+X_{ij}^2}\left[\left(R_{ij}+X_{ij}\right)E_{\mathrm{V},ij,t} + \left(X_{ij}-R_{ij}\right)E_{\theta,ij,t}\right] \end{cases} \tag{A15}$$

$$\begin{cases} \sigma_{\mathrm{P-Q},ij,t} = \dfrac{1}{R_{ij}^2+X_{ij}^2}\sqrt{\left(R_{ij}-X_{ij}\right)^2 D_{\mathrm{V},ij,t} + \left(X_{ij}+R_{ij}\right)^2 D_{\theta,ij,t} + 2\left(R_{ij}-X_{ij}\right)\left(X_{ij}+R_{ij}\right)Cov_{\mathrm{V}\theta,ij,t}} \\ \mu_{\mathrm{P-Q},ij,t} = \dfrac{1}{R_{ij}^2+X_{ij}^2}\left[\left(R_{ij}-X_{ij}\right)E_{\mathrm{V},ij,t} + \left(X_{ij}+R_{ij}\right)E_{\theta,ij,t}\right] \end{cases} \tag{A16}$$

D. Transformation of Substation Capacity Constraints

Based on the circular constraint linearization method, the chance constraint (75) is transformed as follows.

$$\begin{cases} \Pr\left\{-S_{i,\max}^{\mathrm{SUB}} \le \sum\limits_{j\in \mathrm{end}(i)} \tilde{P}_{ij,t} \le S_{i,\max}^{\mathrm{SUB}}\right\} \ge 1-p_{\mathrm{SUB}} \\ \Pr\left\{-S_{i,\max}^{\mathrm{SUB}} \le \sum\limits_{j\in \mathrm{end}(i)} \tilde{Q}_{ij,t} \le S_{i,\max}^{\mathrm{SUB}}\right\} \ge 1-p_{\mathrm{SUB}} \\ \Pr\left\{-\sqrt{2}\,S_{i,\max}^{\mathrm{SUB}} \le \sum\limits_{j\in \mathrm{end}(i)} \tilde{P}_{ij,t} + \sum\limits_{j\in \mathrm{end}(i)} \tilde{Q}_{ij,t} \le \sqrt{2}\,S_{i,\max}^{\mathrm{SUB}}\right\} \ge \\ \quad 1-p_{\mathrm{SUB}} \\ \Pr\left\{-\sqrt{2}\,S_{i,\max}^{\mathrm{SUB}} \le \sum\limits_{j\in \mathrm{end}(i)} \tilde{P}_{ij,t} - \sum\limits_{j\in \mathrm{end}(i)} \tilde{Q}_{ij,t} \le \sqrt{2}\,S_{i,\max}^{\mathrm{SUB}}\right\} \ge \\ \quad 1-p_{\mathrm{SUB}} \end{cases}$$

$$\forall i \in \Omega_{\mathrm{SUB}}, \forall t \tag{A17}$$

The following process is similar to the transformation method of branch thermal constraint in (70)-(74).

REFERENCES

[1] J. Wang, N. Zhou, C. Y. Chung *et al.*, "Coordinated planning of converter-based DG units and soft open points incorporating active management in unbalanced distribution networks," *IEEE Transactions on Sustainable Energy*, vol. 11, no. 3, pp. 2015-2027, Jul. 2020.

[2] H. Gao, L. Wang, J. Liu *et al.*, "Integrated day-ahead scheduling considering active management in future smart distribution system," *IEEE Transactions on Power Systems*, vol. 33, no. 6, pp. 6049-6061, Nov. 2018.

[3] S. He, H. Gao, H. Tian *et al.*, "A two-stage robust optimal allocation model of distributed generation considering capacity curve and real-time price based demand response," *Journal of Modern Power Systems and Clean Energy*, vol. 9, no. 1, pp. 114-127, Jan. 2021.

[4] L. Cheng, N. Qi, L. Wei *et al.*, "Power and energy balance of active distribution network considering operation-control strategy," in *Proceedings of 2018 2nd IEEE Conference on Energy Internet and Energy System Integration (EI2)*, Beijing, China, Oct. 2018, pp. 1-5.

[5] Z. Wu, P. Liu, W. Gu *et al.*, "A bi-level planning approach for hybrid AC-DC distribution system considering $N-1$ security criterion," *Applied Energy*, vol. 230, pp. 417-428, Nov. 2018.

[6] J. Han, N. Liu, and J. Shi, "Optimal scheduling of distribution system with edge computing and data-driven modeling of demand response," *Journal of Modern Power Systems and Clean Energy*, vol. 10, no. 4, pp. 989-999, Jul. 2022.

[7] S. Wang, S. Chen, L. Ge *et al.*, "Distributed generation hosting capacity evaluation for distribution systems considering the robust optimal operation of OLTC and SVC," *IEEE Transactions on Sustainable Energy*, vol. 7, no. 3, pp. 1111-1123, Jul. 2016.

[8] N. Shang, Y. Ding, and W. Cui, "Review of market power assessment and mitigation in reshaping of power systems," *Journal of Modern Power Systems and Clean Energy*, vol. 10, no. 5, pp. 1067-1084, Sept. 2022.

[9] W. Heitkoetter, B. U. Schyska, D. Schmidt *et al.*, "Assessment of the regionalised demand response potential in Germany using an open source tool and dataset," *Advances in Applied Energy*, vol. 1, p. 100001, Feb. 2021.

[10] X. Dai, Y. Li, K. Zhang *et al.*, "A robust offering strategy for wind producers considering uncertainties of demand response and wind power," *Applied Energy*, vol. 279, p. 115742, Dec. 2020.

[11] B. Zhao, H. Qiu, R. Qin *et al.*, "Robust optimal dispatch of AC/DC hybrid microgrids considering generation and load uncertainties and energy storage loss," *IEEE Transactions on Power Systems*, vol. 33, no. 6, pp. 5945-5957, Nov. 2018.

[12] F. Capitanescu, L. F. Ochoa, H. Margossian *et al.*, "Assessing the potential of network reconfiguration to improve distributed generation hosting capacity in active distribution systems," *IEEE Transactions on Power Systems*, vol. 30, no. 1, pp. 346-356, Jan. 2015.

[13] F. Qi, M. Shahidehpour, Z. Li *et al.*, "A chance-constrained decentralized operation of multi-area integrated electricity-natural gas systems with variable wind and solar energy," *IEEE Transactions on Sustainable Energy*, vol. 11, no. 4, pp. 2230-2240, Oct. 2020.

[14] C. Wang, G. Song, P. Li *et al.*, "Optimal siting and sizing of soft open points in active electrical distribution networks," *Applied Energy*, vol. 189, pp. 301-309, Mar. 2017.

[15] Z. Chu, N. Zhang, and F. Teng, "Frequency-constrained resilient scheduling of microgrid: a distributionally robust approach," *IEEE Transactions on Smart Grid*, vol. 12, no. 6, pp. 4914-4925, Nov. 2021.

[16] S. Talari, M. Shafie-khah, F. Wang *et al.*, "Optimal scheduling of demand response in pre-emptive markets based on stochastic bilevel programming method," *IEEE Transactions on Industrial Electronics*, vol. 66, no. 2, pp. 1453-1464, Feb. 2019.

[17] X. Cao, J. Wang, and B. Zeng, "A chance constrained information-gap decision model for multi-period microgrid planning," *IEEE Transactions on Power Systems*, vol. 33, no. 3, pp. 2684-2695, May 2018.

[18] S. Liu, T. Zhang, Z. Lin *et al.*, "Controlled islanding strategy considering uncertainty of renewable energy sources based on chance-constrained model," *Journal of Modern Power Systems and Clean Energy*, vol. 10, no. 2, pp. 471-481, Mar. 2022.

[19] H. Mansy and S. Kwon, "Optimal HVAC control for demand response via chance-constrained two-stage stochastic program," *IEEE Transactions on Smart Grid*, vol. 12, no. 3, pp. 2188-2200, May 2021.

[20] K. Bruninx, Y. Dvorkin, E. Delarue *et al.*, "Valuing demand response controllability via chance constrained programming," *IEEE Transactions on Sustainable Energy*, vol. 9, no. 1, pp. 178-187, Jan. 2018.

[21] M. Salimi, M. Nasr, S. H. Hosseinian *et al.*, "Information gap decision theory-based active distribution system planning for resilience enhancement," *IEEE Transactions on Smart Grid*, vol. 11, no. 5, pp. 4390-4402, Sept. 2020.

[22] M. Ahmadigorji, N. Amjady, and S. Dehghan, "A robust model for multiyear distribution network reinforcement planning based on information-gap decision theory," *IEEE Transactions on Power Systems*, vol. 33, no. 2, pp. 1339-1351, Mar. 2018.

[23] A. Rabiee, A. Soroudi, and A. Keane, "Information gap decision theory based OPF with HVDC connected wind farms," *IEEE Transactions on Power Systems*, vol. 30, no. 6, pp. 3396-3406, Nov. 2015.

[24] A. Soroudi, A. Rabiee, and A. Keane, "Information gap decision theory approach to deal with wind power uncertainty in unit commitment," *Electric Power Systems Research*, vol. 145, pp. 137-148, Apr. 2017.

[25] Y. Zhao, Z. Lin, F. Wen *et al.*, "Risk-constrained day-ahead scheduling for concentrating solar power plants with demand response using info-gap theory," *IEEE Transactions on Industrial Informatics*, vol. 15, no. 10, pp. 5475-5488, Oct. 2019.

[26] J. S. Giraldo, J. A. Castrillon, J. C. López *et al.*, "Microgrids energy

management using robust convex programming," *IEEE Transactions on Smart Grid*, vol. 10, no. 4, pp. 4520-4530, Jul. 2019.
[27] S. E. Hosseini, A. Khajehzadeh, and M. Eslami, "Simultaneous employment of generation rescheduling and incentive-based demand response programs for congestion management in case of contingency," *Journal of Modern Power Systems and Clean Energy*, vol. 10, no. 4, pp. 902-912, Jul. 2022.
[28] S. Cui, Y. Wang, J. Xiao *et al.*, "A two-stage robust energy sharing management for prosumer microgrid," *IEEE Transactions on Industrial Informatics*, vol. 15, no. 5, pp. 2741-2752, May 2019.
[29] R. Argiento, R. Faranda, A. Pievatolo *et al.*, "Distributed interruptible load shedding and micro-generator dispatching to benefit system operations," *IEEE Transactions on Power Systems*, vol. 27, no. 2, pp. 840-848, May 2012.
[30] X. Chen, W. Wu, B. Zhang *et al.*, "Data-driven DG capacity assessment method for active distribution networks," *IEEE Transactions on Power Systems*, vol. 32, no. 5, pp. 3946-3957, Sept. 2017.
[31] H. Yuan, F. Li, Y. Wei *et al.*, "Novel linearized power flow and linearized OPF models for active distribution networks with application in distribution LMP," *IEEE Transactions on Smart Grid*, vol. 9, no. 1, pp. 438-448, Jan. 2018.
[32] P. Pan, *Linear Programming Computation.* Berlin Heidelberg: Springer-Verlag, 2014.
[33] M. Petrelli, D. Fioriti, A. Berizzi *et al.*, "A novel multi-objective method with online Pareto pruning for multi-year optimization of rural microgrids," *Applied Energy*, vol. 299, p. 117283, Jun. 2021.

Shida Zhang received the M. S. degree from the College of Energy and Electrical Engineering, Hohai University, Nanjing, China, in 2018. He is currently working toward the Ph.D. degree with the School of Electrical and Information Engineering, Tianjin University, Tianjin, China. His research interests include optimal planning and operation of distribution system.

Shaoyun Ge received the M.S. degree from the School of Electrical Engineering and Automation, Tianjin University, Tianjin, China, in 1991, and the Ph. D. degree from Hong Kong Polytechnic University, Hong Kong, China, in 1998. He is currently a Professor with the School of Electrical and Information Engineering, Tianjin University, Tianjin, China. His research interests include distribution system planning, power distribution reliability, and electric vehicles.

Hong Liu received M.S. and Ph.D. degrees from the School of Electric Automation Engineering, Tianjin University, Tianjin, China, in 2005 and 2009, respectively. He is currently a Professor with the School of Electrical and Information Engineering, Tianjin University, Tianjin, China. His research interests include optimal planning and operation of distribution system and integrated energy system.

Junkai Li received the M. S. degree in 2021 from the School of Electrical and Information Engineering, Tianjin University, Tianjin, China, where he is currently working toward the Ph.D. degree with the School of Electrical and Information Engineering in Tianjin University, Tianjin, China. His research interests include optimal planning and design of distribution system.

Chenghong Gu received the bachelor's degree in electrical engineering from Shanghai University of Electric Power, Shanghai, China, in 2003, the master's degree in electrical engineering from Shanghai Jiao Tong University, Shanghai, China, in 2007, and the Ph. D. degree from the University of Bath, Bath, UK, where he is currently a Reader and an EPSRC Fellow with the Department of Electronic and Electrical Engineering. His major research interests include multivector energy system, smart grid, and power economics.

Chengshan Wang received the Ph. D. degree in electrical engineering from Tianjin University, Tianjin, China, in 1991. Currently, He is a Professor with the School of Electrical and Information Engineering, Tianjin University, where he is also the Director of the Key Laboratory of Smart Grid of the Ministry of Education. He is an Academician of Chinese Academy of Engineering. His current research interests include analysis and planning of distribution system, distributed generation systems and microgrid, and power system security analysis.